TECHNICAL REPORT BRL-TR-3096

BRL

LASER INDUCED IR FLUORESCENCE SPECTRA OF SIMULANT CHEMICAL THREAT AGENT AND EXHAUST VAPORS

ROBERT B. BOSSOLI
GEORGE M. THOMSON

APRIL 1990

U.S. ARMY LABORATORY COMMAND

BALLISTIC RESEARCH LABORATORY
ABERDEEN PROVING GROUND, MARYLAND

NOTICES

Destroy this report when it is no longer needed. DO NOT return it to the originator.

Additional copies of this report may be obtained from the National Technical Information Service, U.S. Department of Commerce, 5285 Port Royal Road, Springfield, VA 22161.

The findings of this report are not to be construed as an official Department of the Army position, unless so designated by other authorized documents.

The use of trade names or manufacturers' names in this report does not constitute indorsement of any commercial product.

REPORT DOCUMENTATION PAGE

Form Approved
OMB No. 0704-0188

1. AGENCY USE ONLY (Leave blank)	2. REPORT DATE	3. REPORT TYPE AND DATES COVERED
	April 1990	

4. TITLE AND SUBTITLE
Laser Induced IR Fluorescence Spectra of Simulant Chemical Threat Agent and Exhaust Vapors

5. FUNDING NUMBERS
PE: 61102A
PR: 1L161102AH
TA: 43

6. AUTHOR(S)
Dr. Robert B. Bossoli and Dr. George M. Thomson

7. PERFORMING ORGANIZATION NAME(S) AND ADDRESS(ES)
U. S. Army Ballistic Research Laboratory
ATTN: SLCBR-TB-D
Aberdeen Proving Ground, MD 21005-5066

8. PERFORMING ORGANIZATION REPORT NUMBER
BRL-TR-3096

9. SPONSORING / MONITORING AGENCY NAME(S) AND ADDRESS(ES)
U. S. Army Ballistic Research Laboratory
ATTN: SLCBR-DD-T
Aberdeen Proving Ground, MD 21005-5066

10. SPONSORING / MONITORING AGENCY REPORT NUMBER

11. SUPPLEMENTARY NOTES

12a. DISTRIBUTION / AVAILABILITY STATEMENT
Approved for public release; distribution unlimited.

12b. DISTRIBUTION CODE

13. ABSTRACT *(Maximum 200 words)*

Infrared (IR) fluorescence spectra have been measured for several agent/exhaust simulants illuminated by a slowly (10-200 Hz) chopped infrared laser. The vapor and vapor-air mixtures exhibit fluorescence at wavelengths corresponding to their infrared absorption spectra when excited by a grating tuned 5 watt CO_2 (9 - 11 μm) laser. Utilizing a calibrated spectral measurement apparatus, the spectra are presented in terms of the actual quantity of fluorescence energy emitted from a unit volume of vapor and wavelength span for a given set of excitation conditions (laser wavelength, power, and chop frequency) and simulant pressure. The addition of air to small quantities (10 - 30 Torr) of the simulants quenches, but does not completely extinguish, the fluorescence. A linear increase in the infrared fluorescence intensity with laser chopping period is observed along with very slow (msec) rise and decay times of the fluorescence signal. These observations are attributed to the bulk heating of the vapor or vapor-air mixture along the laser beam path due to the slow chopping frequencies. These results indicate the possible utilization of laser-induced infrared fluorescence in remote sensing of chemical vapors of interest to the Army (agents/vehicle exhausts).

14. SUBJECT TERMS
Infrared Fluorescence; Agents; Spectral measurements; Similants; Laser-induced; Chemical Sensing; IR Spectra; Remote Sensing

15. NUMBER OF PAGES
66

16. PRICE CODE

17. SECURITY CLASSIFICATION OF REPORT	18. SECURITY CLASSIFICATION OF THIS PAGE	19. SECURITY CLASSIFICATION OF ABSTRACT	20. LIMITATION OF ABSTRACT
UNCLASSIFIED	UNCLASSIFIED	UNCLASSIFIED	UL

INTENTIONALLY LEFT BLANK.

TABLE OF CONTENTS

INTENTIONALLY LEFT BLANK.

LIST OF FIGURES

ACKNOWLEDGMENTS

The authors are grateful to the Oriel Corporation for providing detailed data on the calibration of their monochromators and light sources and for permission to incorporate some of their artwork into Figure 2.

1. INTRODUCTION

1.1 Background. The application of laser techniques for remote sensing of chemical threat agents has been investigated for many years. The two most thoroughly examined methods, Differential Absorption Lidar (DIAL) and Differential Scattering Lidar (DISC),[1] use the absorption and the scattering of transiting infrared (IR) beams to deduce information about an aerosol's concentration and composition. Both methods, however, suffer drawbacks--requiring some sort of reflector (DIAL) or detailed a priori knowledge of scattering properties for quantitative assay (DISC). Nonetheless, DIAL and DISC represent what are to date the most promising approaches as evidenced by both lab and field studies. Other remote sensing schemes have shown some success including Raman Scattering and visible/ultraviolet laser-induced fluorescence.[2,3,4,5]

Among the least studied of laser techniques is another fluorescence method, one which operates in the IR. Originally considered for remote sensing of atmospheric carbon monoxide by Kildal and Byer,[6] sensing via infrared fluorescence (IRF) hinges upon two phenomena observed where an IR laser beam crosses an air-vapor mixture: first, that energy is preferentially absorbed from the beam if the laser is tuned to a specific wavelength which resonately excites one of the vapor molecule's vibro-rotational transitions, and second, that some of the absorbed energy is reradiated at other IR wavelengths characteristic of the vapor. Remote sensing utilizing IRF would involve irradiating the target region with an appropriately tuned IR laser and then searching for correlated emissions induced at other IR wavelengths.

In their pioneering paper, Kildal and Byer predicted laser-induced IR fluorescence's range sensitivity for short pulse excitation and compared it with the other laser techniques just mentioned. A related review paper by Robinson and Dake covers some of the research around this same time period and also suggests and investigates the possible use of IRF in remote sensing of organic atmospheric pollutants.[7] The paper reviews much of the work by its authors and their coworkers on many organic compounds, with the most detailed attention centered on ethylene gas. In that case, using a slowly chopped CO_2 laser and wide IR bandpass filter/detectors, they were able to detect IRF emissions from mixtures containing a low percentage of the ethylene in 1 atm of nitrogen. These accomplishments notwithstanding, laser-induced IRF has found its widest use to date as a technique in which pulsed CO_2 lasers are employed to investigate collisional lifetimes and inter/intra-molecular energy transfer of molecules. One of several reviews of the applications of IRF has been given by Bailey and Cruickshank.[11] In light of these studies, IR fluorescence's application to military problems seemed both tantalizing and challenging. Consequently, we undertook a simple modeling study of IR fluorescence's possible use in a remote sensing system for various military aerosols such as toxic threat

agents and vehicle exhausts. These calculations, although limited by available experimental data, indicate that systems of reasonable size could be built that would possess sufficient sensitivity to detect and quantitatively measure the concentration of dilute aerosols at useful (1-5 km) distances. During the course of our work, we became aware of a similar ongoing theoretical study by Bernstein, et al., funded by the Army Chemical Research Development and Engineering Center (CRDEC). The resulting CRDEC report also concluded that laser-induced IRF held promise as a remote sensing technique for two particularly important substances, G and V threat agents.[12]

Unfortunately, all the above modeling studies suffer a common shortcoming--the lifetimes for the key processes that these complex molecules undergo are derived from short-pulsed (<1 μsec) laser-induced IRF measurements limited to the simple diatomic and triatomic molecules. These lifetimes were then extrapolated to more complex cases at hand by use of their respective IR absorption cross sections. No actual quantitative IRF results on the higher molecular weight vapors, especially chemical threat agents or their simulants, are available. The extrapolations indicate that nonradiative de-excitation pathways (in particular, collisions) are very numerous and possess rates that would compete strongly with the fluorescence processes, especially in dilute air-vapor mixtures. If the competition does indeed scale in this fashion, one may conclude that fluorescence would, in effect, be "quenched" to the extent that systems based upon it would not exhibit the sensitivity of other laser techniques like DIAL and DISC. It appears that questions such as these have stymied beforehand any extension of IRF to sensing problems involving complex molecules. This pessimism is contradicted by the work of Robinson and his coworkers previously mentioned. Their results suggest that excitation by a slowly chopped or pulsed CO_2 laser may produce sufficient IRF for remote detection with sensitivity comparable to that of the other laser techniques. If these observations are borne out by further investigation, it appears that other mechanisms are at work which may have pivotal consequences in the further development and exploitation of laser-induced IRF.

1.2 The Present Program. It is the premise of this research that, given the lack of basic, quantitive data on the IRF properties of more complex molecules (especially for slow-chopped laser excitation) and the recent improvement in IR lasers/detectors/instrumentation, IRF should be investigated in more detail for possible use in military roles. Among such roles are the remote sensing of threat agents and the gathering of battlefield intelligence from vehicle exhausts. Accordingly, we initiated measurements of those key parameters important in empirically validating laser-induced IRF for remote detection. The potential payoff of detection via laser-induced IRF would be a means that is intrinsically less complex, smaller, more widely applicable, and operationally more flexible than other laser-based remote sensing schemes.

The following report is the first in a series that details the results of our IRF studies on compounds that are used to simulate target vapors of military interest. In this report, the spectral features of the fluorescing vapor will be presented in quantitative form--that is, in terms of the absolute amount of fluorescent energy given off over a given wavelength span under specified excitation conditions. It is the first time, to the best of our knowledge, that such photometric measurements of IRF have ever been reported. Data will also be presented on the consequences of atmospheric quenching and on the effect of the duration of the illuminating laser beam. Taken together, these data provide insights into the physical processes and mechanisms that produce fluorescence and cause it to be curtailed.

The second report is geared toward assessing the potential of fluorescence for exploitation. The data of the first report are supplemented with a detailed study of fluorescence's dependence upon both laser power and vapor partial pressure in the atmosphere. From this foundation, one can model the response of various possible IRF-based remote sensing systems for different ranges, target aerosol concentrations, and depths. The results indicate that the amount of IRF, even after the effects of dilution and quenching are factored in, is more than sufficient to justify continued interest in IRF and that sensing systems with ranges of hundreds of meters at least can be built with fairly modest, commercially available hardware.

The last report in this series, reporting experiments that, at this writing, are only being assembled, will detail our attempts to verify the predictions in the field. It is expected that at the conclusion of this program a solid judgment can be made on the likelihood that a tactically useful IRF remote sensing system can be successfully developed.

2. EXPERIMENTAL

2.1 Fluorescence Apparatus. A fluorescence spectral measurement apparatus (illustrated in Figure 1) was constructed to investigate laser-induced IRF of selected agent and exhaust simulant vapors. The device provides for several functions needed to carry out our evaluation including delivering a monochromatic (laser) beam to a target aerosol of known properties, defining geometrically the beam-target interaction region, and, finally, analyzing the fluorescent IR output. The exciting IR beam comes from a 5-W, grating-tuned (9.2 to 10.8 μm), CO_2 waveguide laser that delivers a 1.5 mm diameter (at exit full-width to $1/e^2$ points) beam with an 8.8-mrad divergence. While traversing the 60-cm distance from the laser output window to the chamber entrance window, the beam passes through a variable frequency optical chopper and, in some instances, an absorption chamber. The combination of these two assemblies allows one to modulate the beam with a selected frequency square

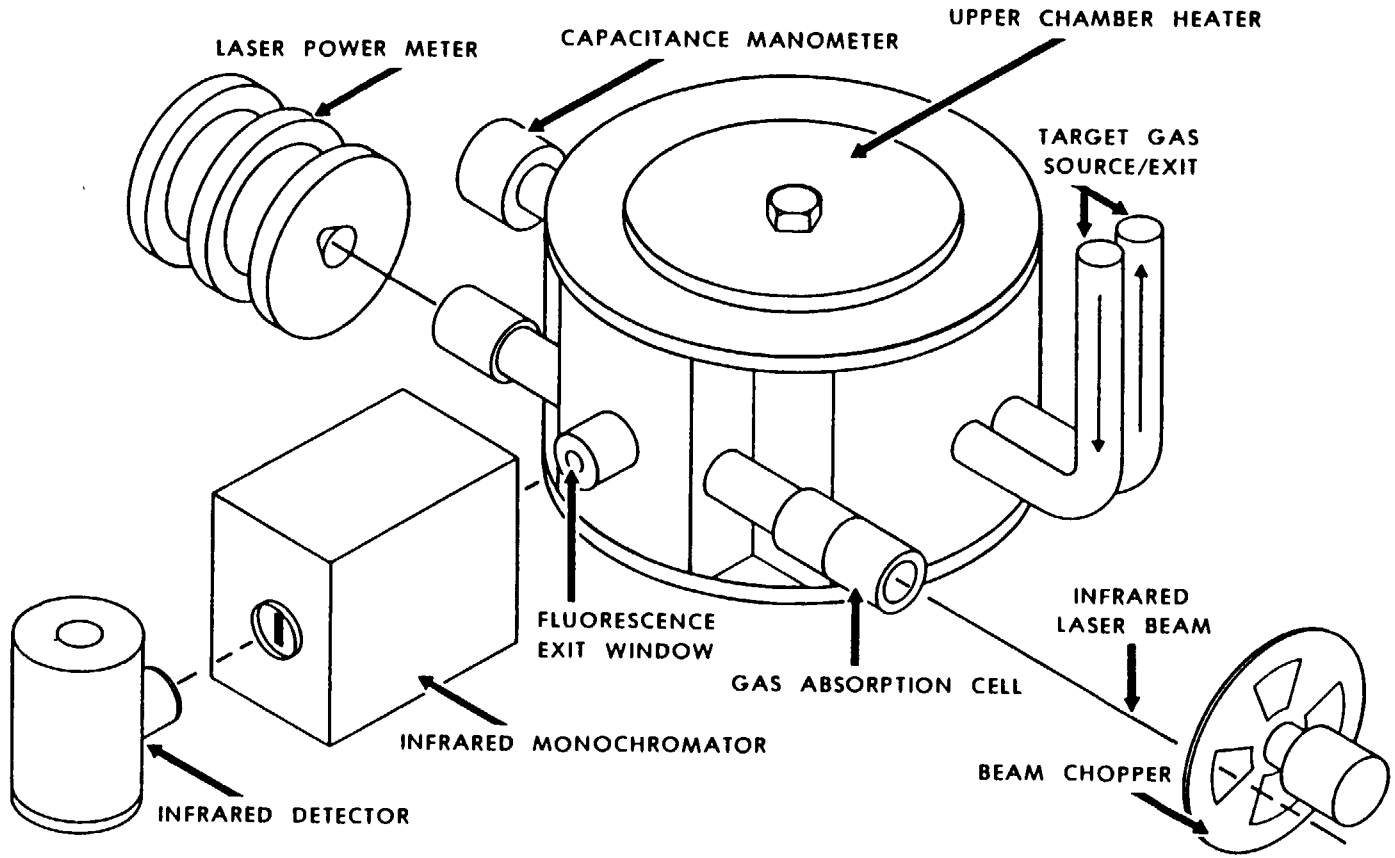

Figure 1. The IR fluorescence spectral measurement system.

wave and adjust its intensity to any desired power level. A laser power meter head (not shown) can be interposed in the beam path prior to entering and exiting the chamber, allowing the laser output to be measured prior to and after its passage through the vapor.

The beam-vapor interaction region lies within a 17-cm-diameter cylindrical, aluminum chamber that is fitted with ZnSe windows (antireflection coated for 10.6-μm transmission) through which the laser beam enters and departs. This arrangement provides an 18-cm-long path through the vapor along a recess cut along a chord tangent to the chamber's circular interior wall. The same wall also includes ports for measuring vapor pressure with thermocouple gauges and capacitance manometers, introducing the simulant vapor, and for evacuating its contents via a mechanical vacuum pump to below 0.02 Torr. The vapor inlet port connects to an independently heated injection cell that allows carefully metered quantities of simulant to be admitted to the main chamber through a variable-orifice valve. Temperature-controlled heater disks (attached on the top and bottom surfaces of the chamber) keep the simulants that are contained within vaporized (if needed) at temperatures up to 373°K. If vapors require the highest chamber temperatures (>333°K), then the capacitance manometer's special high-temperature sensing head may be heated in order to insure that no condensation of the simulant vapors affects its operation. Thermocouples attached to the main chamber, the injection cell, and the manometer head closely monitor all these critical temperatures. Even so, high-temperature operation with the less-volatile simulants introduces some uncertainty into the chamber pressure due to small (±3°K) temperature fluctuations in the chamber and capacitance manometer head.

The task of spectrally observing the IRF leaving the interaction region was carried out with either of two means--a simple IR interference filter or an Oriel compact (1/8 meter, f/3.7) monochromator with a grating blazed at 8 μm. The latter device has its axis directed at right angles to the beam path and viewed a precisely measured volume of the fluorescing region through a ZnSe window. The distance from the beam to the window is kept short (12 mm) to minimize re-absorption of the fluorescence at higher pressures. In this configuration the IRF flux entered the monochomator through its adjustable entrance slit (0-3.2 mm) oriented parallel to the beam direction. The total separation from the laser beam path in the chamber through the window to the monochromator entrance slit was 3.75 cm.

The unfocused IRF flux emerging at the exit of the monochromator illuminated a liquid nitrogen cooled, 1-mm square, HgCdTe IR detector (Judson Infrared Inc., Model J15-D12). If the IR falls within the wavelength range of 4 to 14 μm, the biased detector responds with a current. Its response peaks (at a wavelength λ_p) in the 10- to 11-μm region with a detectivity D*(@10 kHz, λ_p) of 3.4 x 10^{10} cm-$Hz^{1/2}$/W. The detector's associated AC coupled preamplifier provides both the bias and initial gain of 54 dB to the photocurrent over a frequency bandwidth of 5 Hz to 10 MHz. The

output signal next receives an additional 20-dB gain via an Ithaco model 165 preamplifier, frequency preselection by a low-pass (4 kHz) filter, and lock-in amplification from a Ithaco 391A lock-in amplifier referenced to the chopping frequency. For the spectral scans, the voltage outputs both of the lock-in amplifier and monochromator's wavelength readout are digitized by Keithley 179A digital voltmeters and sent over IEEE-488 interfaces to a Tektronix 1164 (Digital Equipment Inc. PDP-11/34) computer for subsequent storage and processing.

2.2 Calibration of System. The evaluation of IR fluorescence's usefulness in a remote sensing role requires a measurement of the fluorescent spectral radiance as a function of illuminating wavelength and power and other critical parameters. In order to get the quantitative results needed for this determination, various factors such as detector and monochromator spectral response, throughput, and the fluorescent gas pressure/geometry need to be determined and held fixed.

The monochromator-detector combination was calibrated for the spectral response and throughput by coupling it to a SiC glowbar "gray-body" IR source mounted inside an Oriel model 7340 illuminator. The source provides an IR flux with a known black-body-like (800°K to 1,200°K range) spectral irradiance curve focused onto the entrance slit of the monochromator. By measuring the output amplified detector signal, it then becomes a straight-forward matter to calculate corrections for the nonlinear spectral response of the monochromator-detector system. The overall layout of the calibration apparatus is shown in Figure 2.

The first step in the calibration was determining the operating temperature of the glowbar IR source as the voltage applied to it was incrementally changed over a 10- to 14-volt range. At each step, the temperature was measured using a IRCON two-color, optical pyrometer (range 973°K to 1,673°K). The resulting temperature versus applied voltage curve for the glowbar appears in Figure 3. The SiC resistor glowbar has an average emissivity of 0.88 in the IR (1 to 14 μm).[13] Under the operating conditions selected for the calibration (T = 1,073°K), it was possible to compute the value of the glowbar spectral radiance from data provided by its manufacturer.[14] The glowbar was adjusted to the calibration temperature, and a concave mirror in the illuminator focused the emissions from its 6.2 x 20 mm active region into a magnified image (1.8X) at the monochromator entrance slit. A chopper, interposed between the illuminator and the monochromator, modulated the IR, which the compact monochromator spectrally analyzed and directed onto the HgCdTe detector. Scans of the glowbar's IR output between 4 and 14 μm were obtained using 0.6- and 0.3-mm slit widths and chopping at 200 Hz. The two slit widths provide approximate bandpasses of 0.061 and 0.03 μm, respectively. Figure 4 shows the 0.061-μm bandpass data for the 1,073°K gray-body glowbar source with the lock-in amplifier output in millivolts plotted against the monochromator wavelength in microns.

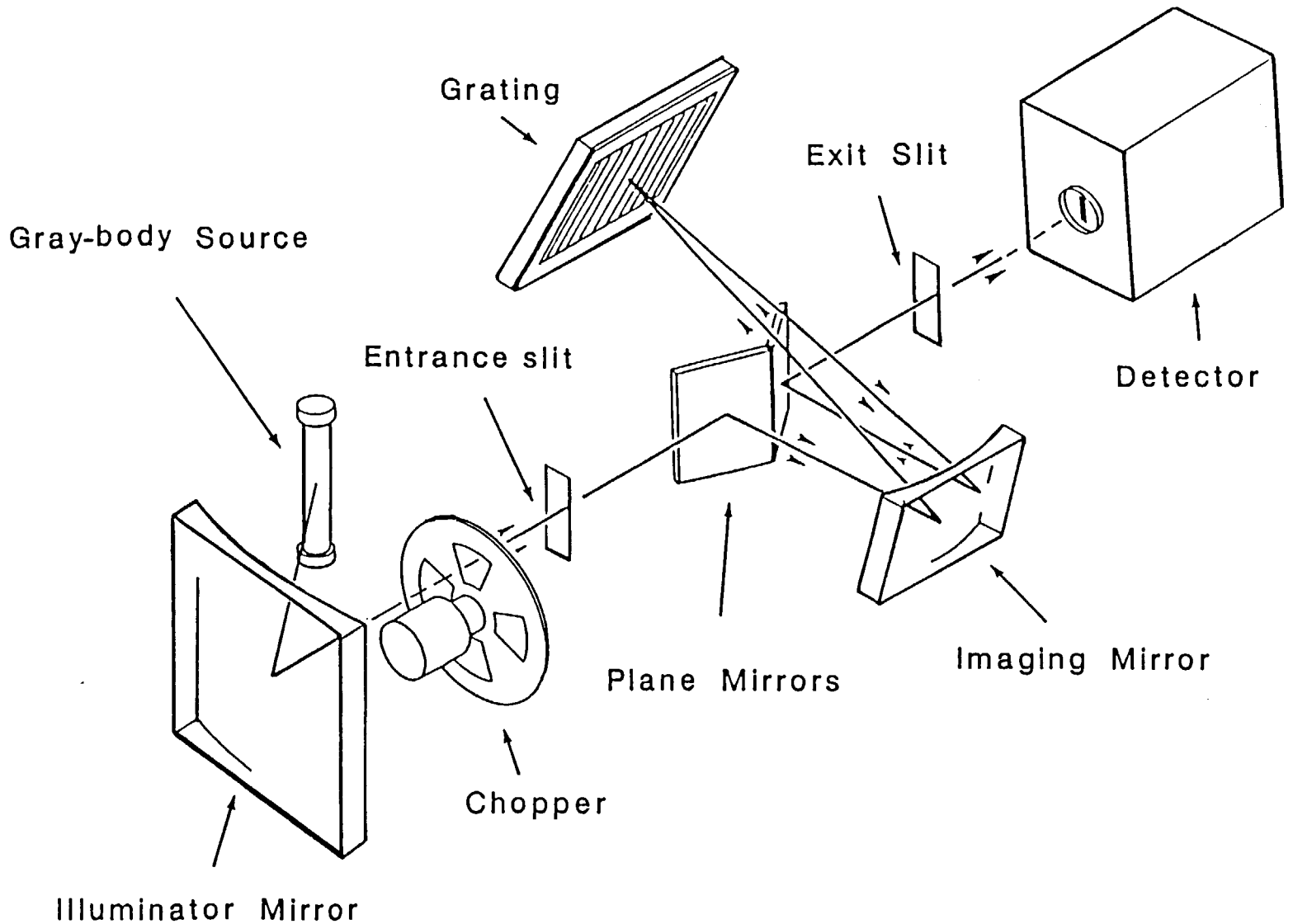

Figure 2. The apparatus for calibrating the measurement system response.

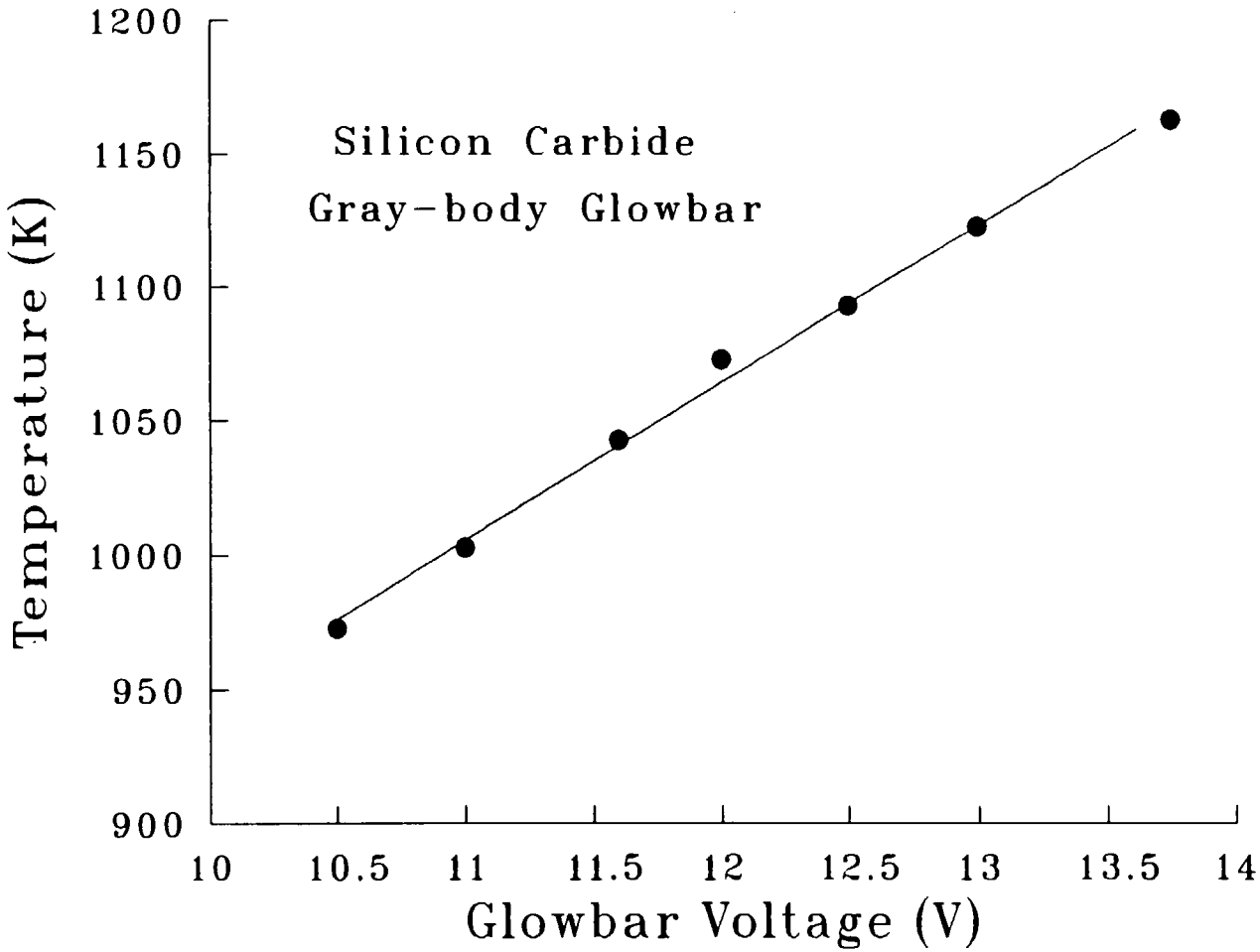

Figure 3. Calibrating glowbar temperature versus applied voltage.

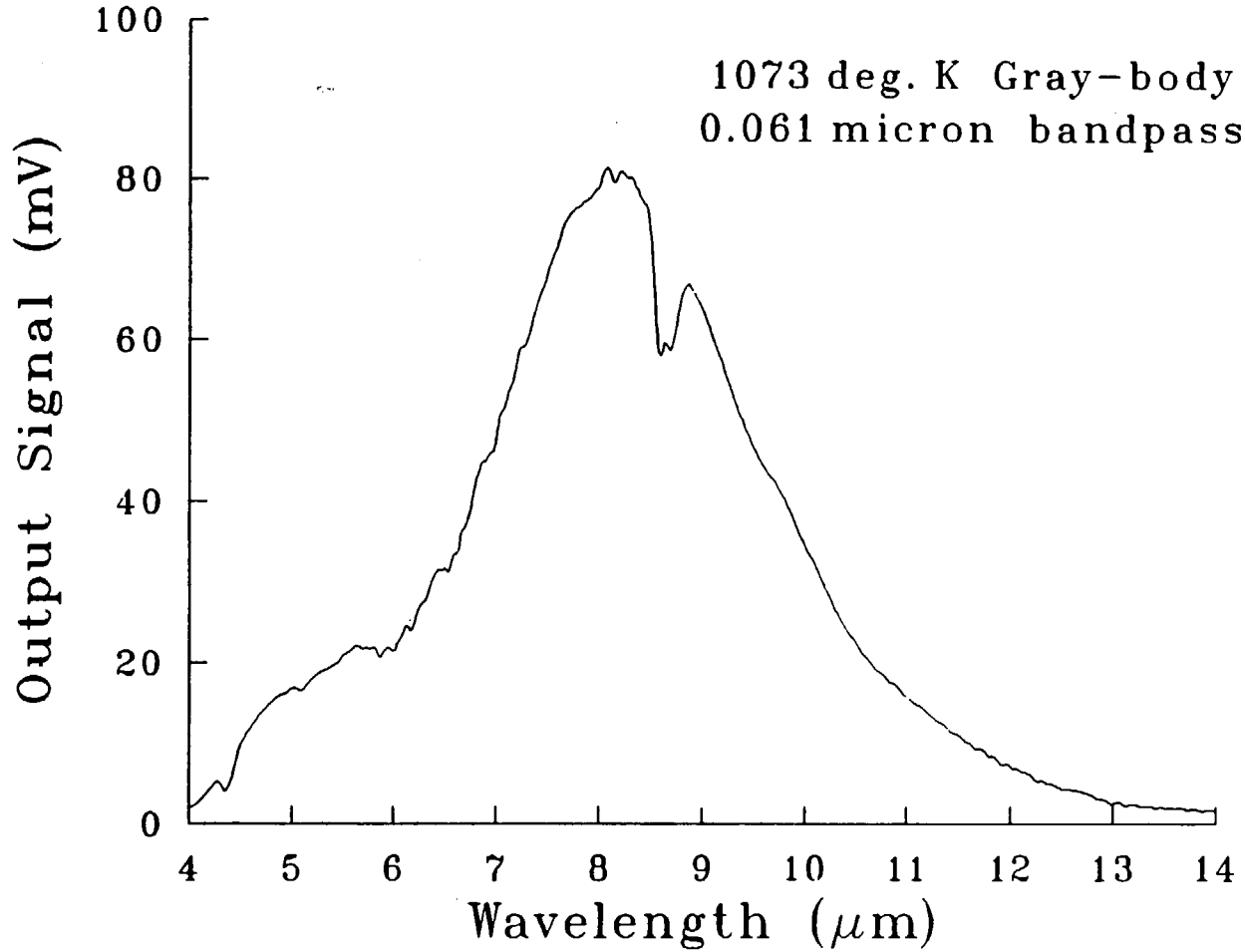

Figure 4. Raw spectrum of the glowbar at a temperature 1,073°K, taken with the monochromator set for a 0.061 μm bandpass.

Combining the aforementioned values of the glowbar spectral irradiance with the known throughput of the various devices at 8 μm,[14] it was then possible to calculate the spectral radiant power expected at 8 μm through both the entrance and exit slits of the monochromator for this illuminator-monochromator combination with 0.061-μm bandpass. Details of the method of calculation are given in Appendix A. Its result allows us to relate, at these single values of wavelength and bandpass only, a measured lock-in amplifier output in millivolts with the corresponding spectral radiant power at the input slit of the monochromator. To extend this result to other wavelengths, we assume that the glowbar is a 1,073°K gray-body, and we can use Planck's law to describe its spectral distribution curve or:

$$W_B = \frac{3.745 \times 10^4}{\lambda^5} [1/(e^{1.438 \times 10^4/\lambda T} - 1)] \quad (1)$$

where W_B is the radiant IR flux per unit area per unit wavelength at a specified wavelength (in microns) and absolute temperature T (°K). The spectral power incident on the front slit at any wavelength may then be ascertained by normalizing this unique curve to the value we have calculated at the 8-μm point. In the present case, these calculations are all carried out in a computer program--a program which calculates the Planck's law curve, normalizes it to the 8-μm point, compares the result to the "raw," digitized gray-body lock-in amplifier output data (Figure 4) at each wavelength, and produces a calculated correction factor function for wavelengths between 6 and 14 μm. The wavelength dependence of the correction factor is shown in Figure 5 displayed in arbitrary units.

A second program has also been written to apply the above correction curve to any raw lock-in spectral data in order to correct it for instrumental response. When this program is exercised in a circular fashion on the raw data from the glowbar gray body shown in Figure 4, consistency demands that a Planck's law-type spectral power curve be produced, and, furthermore, that the curve derived from the data and one directly from Planck's law agree at all wavelengths. This can be confirmed by examining the value at 8 μm, the spectral power value used to normalize the curve. The reproduced spectral power curve appears in Figure 6 and has the desired value of 23 μW/μm (as calculated in Appendix A) at that wavelength.

Further independent verifications of this calibration are also described in Appendix A; one is based on the responsivity of the HgCdTe detector provided by its manufacturer, another upon a separate measurement using an Oriel 7080 pyroelectric radiometer. All demonstrate that the method incorporated into the program can indeed convert values of the lock-in amplifier output voltage (in millivolts) to the corresponding spectral radiant power entering the slit of the monochromator P_s in units of milliwatts/microns.

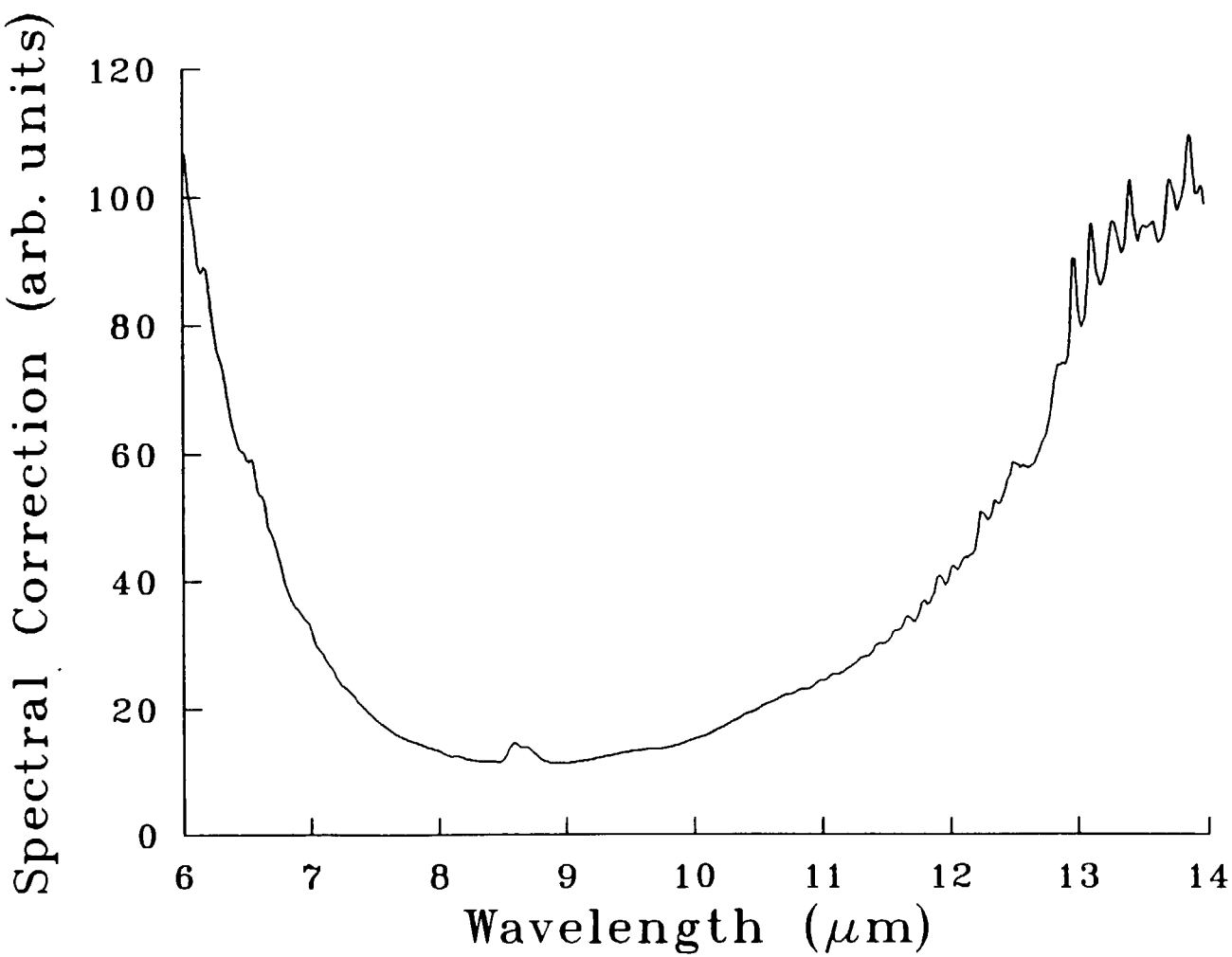

Figure 5. Spectral correction factor (arbitrary units) determined from the raw data in Figure 4 and a 1,073°K gray-body (glowbar) calculated curve.

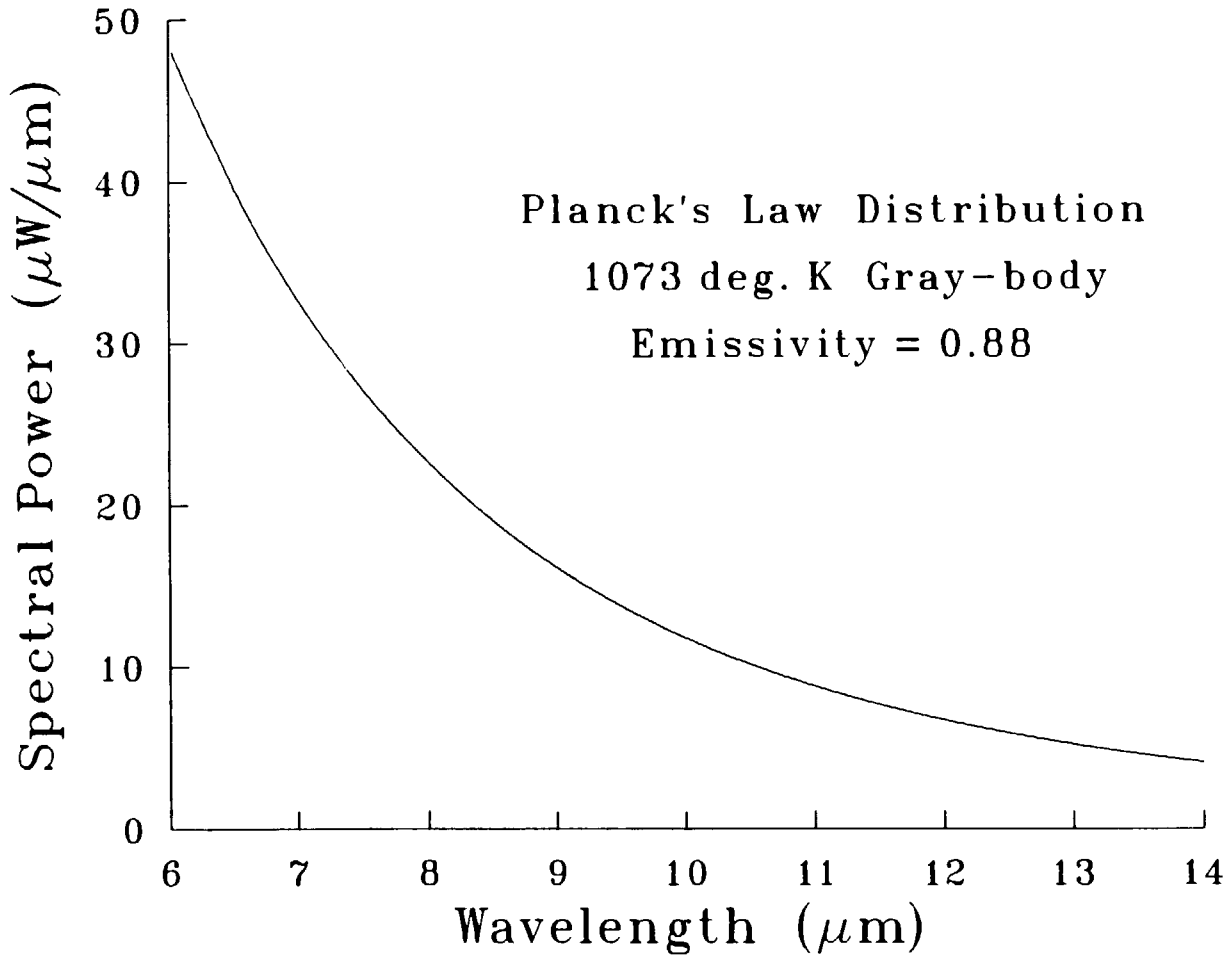

Figure 6. Power spectrum of IR emissions from the glowbar passing through the monochromator entrance slit from 6 to 14 μm. Data are corrected from monochromator-detector response factors.

One final factor must be taken into account--the geometry of the fluorescing volume in front of the entrance slit of the monochromator. This is calculated in Appendix B for the present case, specifically a laser beam whose diameter at the segment in front of the monochromator has expanded to 5 mm. In our apparatus, the entire column of vapor lying in the beam's path with the chamber fluoresces. However, the apparatus only detects emission from volume of the segment seen by the monochromator as defined by the slit aperture and the speed of the monochromator imaging mirror (f/3.7). The fluorescing column of vapor's intersection with the cone of view of the monochromator and the distance from the gas to the entrance slit (see Figure 1, Appendix B) together determine that factor needed to convert spectral power at the entrance slit P_s to the volume spectral radiance of the fluorescing vapor column in milliwatts/(microns - steradian - cubic centimeters), i.e.,

$$\Re_\lambda = \frac{2789}{d(mm)} \cdot P_s \, . \tag{2}$$

This second correction factor was also incorporated into the computer program and produced the corrected spectral fluorescence data presented in this report. These spectra constitute one of the critical factors in determining the feasibility of using IRF for remote sensing.

3. PROCEDURES AND PERFORMANCE

3.1 General. The basic data elements obtained in this effort were the spectra of IR fluorescence emissions coming from gases of known composition and partial pressure, illuminated by a laser beam having known size, power, and wavelength. The calibration procedure just described was used to put the emissions detected on a quantitative footing.

3.2 Operating Procedures. At the start of each spectral data-taking session, approximately 10 cm^3 of simulant liquid was introduced to the small injection cell. The temperature controllers were turned on, and both the injection cell and IRF chamber were allowed to come to equilibrium at the temperature chosen to keep the simulant vaporized. Typical chamber temperature set point values were 323°K - 333°K for Freon and methyl alcohol, and 353°K - 363°K for DMMP. Ethylene, a gas at standard temperature and pressure (STP), was introduced directly into the IRF chamber, and measurements were performed at room temperature. During the chamber warm-up, the laser was also tuned to the desired excitation wavelength and allowed to stabilize.

A mechanical vacuum pump was used to evacuate the IRF chamber to a pressure below 20 mTorr. Laser beam power was measured before and after traversing the 18-cm path within the chamber in order check the alignment and other factors affecting its intensity (window transparency, etc.). A small amount of simulant vapor was thereupon introduced into the main chamber to purge the connecting lines of any air present, and the chamber was repumped down. While carefully monitoring the chamber pressure with a capacitance manometer, the desired amount of simulant vapor was added to the main chamber (typical amounts fell in the 1- to 100-Torr range). The vapor's presence reduced the transmitted beam power, as measured with the power meter located behind the exit window of the chamber. Large pressures of simulants could completely absorb the laser power when the laser was operating at a wavelength where the vapor exhibits large absorption. A quantitative comparison of the beam power before and after the admission of the gas allows one to estimate the simulant vapor's absorption coefficient at the laser wavelength. From that comparison, one may infer the beam energy absorbed not only over the entire path in the chamber but also over that portion of the path within the monochromator's field of view.

Having determined the vapor's absorption of the laser output, the monochromator was adjusted to a wavelength away from the laser's where the fluorescence was most intense, and the lock-amplifier's sensitivity, phase, and time constants were optimized for best output. The monochromator was then set to a wavelength below the desired starting wavelength, and its wavelength scanning motor was started. The 1134 computer, running a spectral digitizing program, began recording IRF data when the desired starting wavelength was reached. The IRF data (the voltage output from the lock-in amplifier and the corresponding monochromator wavelength) were logged each time a programmed wavelength interval (usually 0.02 μm) elapsed until the ending wavelength of the spectral scan was reached. The computer finally plotted out this raw spectral data and stored it on a magnetic disk for later correction.

In the course of this study, numerous spectra were acquired, systematically spanning several different values of laser wavelengths and laser powers over a wide range of vapor pressures--all for the purpose of detecting interesting, exploitable trends and phenomena. The specific spectra presented below, unless otherwise noted, were recorded at those vapor pressures where the greatest fluorescence output took place. In most cases, the monochromator slits were set wide open (3.2 mm) which gave a 0.32-μm bandpass. Data taken at smaller slit widths did reveal some finer structure present in the fluorescence spectra that correlated with details present in the absorption spectra of the simulants. For remote sensing use, however, the general character of the broad spectral features and their relative intensities are of greater interest.

The somewhat broad monochromator resolution utilized in obtaining the IRF spectra presented in this report is demonstrated in Figure 7. This figure contains two spectral scans taken with no gas present in the chamber and with the laser operating at the two wavelengths used to produce IRF. The flux detected in this case is pure, scattered laser light (monochromatic IR), and the apparent width of this peak is almost completely due to instrumental effects of the fairly wide bandpass (0.32 μm). It should also be noted that the signal processing/detection method used in this experiment, lock-in amplification, discriminates against scattered laser light. We find that fluorescence waveforms do not resemble those of the incident beam (a chopped squarewave), while scattered laser light does. The waveforms in Figure 8 illustrate such behavior; the first represents the incident waveform (unsymmetrically chopped laser); the next four are IRF waveforms taken under a variety of conditions. Note the apparent integration of these signals resulting from very slow (msec) rise and decay times. This results in a phase shift between the exciting laser and the IRF waveforms. The origin of the signal integration provides a clue to the nature of the fluorescence process and will be discussed in Section 5. The phase-sensitive nature of the lock-in amplifier limits the scattered/reflected signals presence in the measured spectra, leaving, at worst, a readily identified artifact.

The 1-Torr pure vapor data shows the signature of another important effect--saturation. Saturation takes place when the laser beam apparently depletes the population of vapor molecules in certain states essential to the absorption (and, therefore, fluorescence) process. As a result, longer laser illumination time cannot increase the number of excited molecules contributing to the fluorescent output. This behavior occurs under conditions of small vapor pressures and very slow chopping rates (that is, long laser illumination periods). Other observations and discussions of these phenomena will be made in Sections 4.6 and 5.

4. IR FLUORESCENCE SPECTRA

4.1 Freon (Freon 113, $C_2Cl_3F_3$). As a starting point in studying the fluorescence spectrum of a vapor, one should consider what is essentially its inverse, the absorption spectrum. One such IR absorption spectrum, for Freon smear,[15] is shown in Figure 9. Several peaks in the 5- to 15-μm wavelength range are evident. Compare this to the IRF spectrum of Freon shown in Figure 10, which was acquired when the methods above were applied to 30 Torr of Freon excited with a laser at 10.76 μm. It can be seen that the IRF spectrum mimics the IR absorption spectrum, indicating that the absorbed laser power has been redistributed among the various vibro-rotational modes of the Freon molecule. Note also that absorption and fluorescence peaks depicted in Figures 9 and 10 respectively occur at identical wavelengths (8.5, 9.1, 9.6, 11.3, and 12.3 μm). The similarities become even more striking when the raw fluorescence data are corrected for spectral response via the computer program

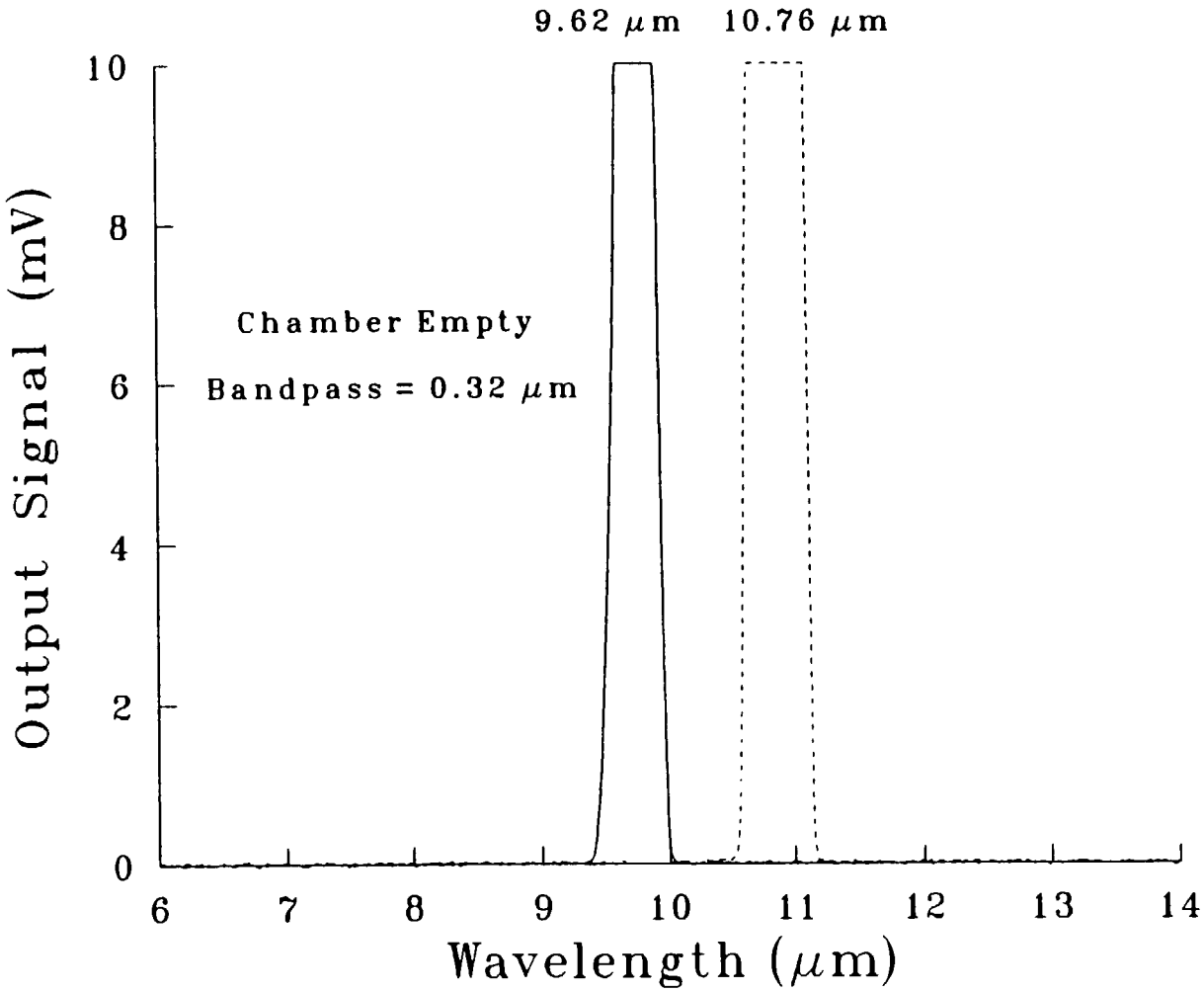

Figure 7. The IR spectra acquired when lasers beams at 10.76 μm (dashed) and 9.62 μm (solid) are directed at the chamber while it is empty of gas.

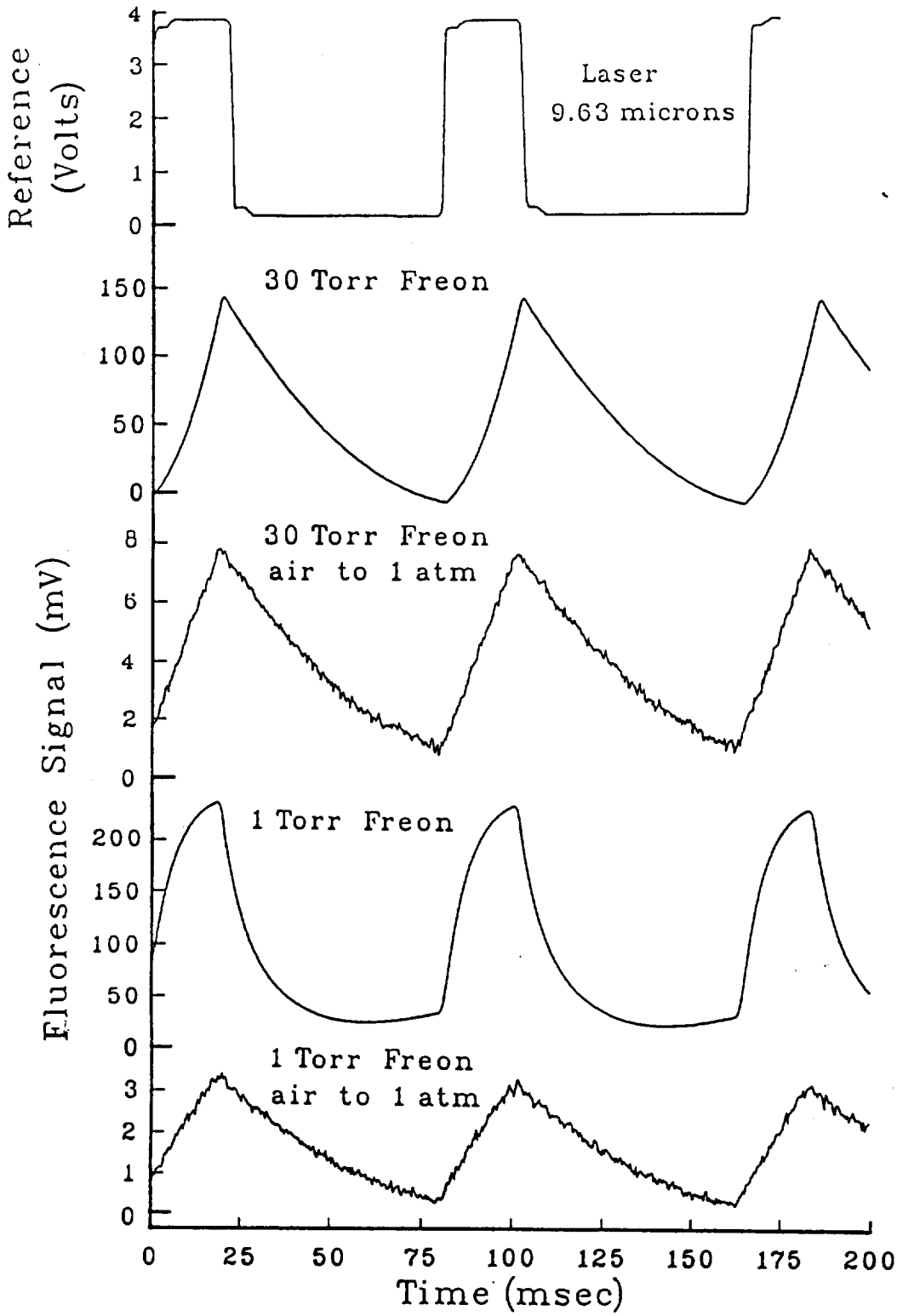

Figure 8. Waveforms of the detected IRF signal illustrating the response when various combinations of gases are present in the chamber. Note the effect of saturation with 1 Torr of Freon. The upper curve shows the waveform of the incident beam which was chopped asymmetrically - 22 msec-on/66 msec-off.

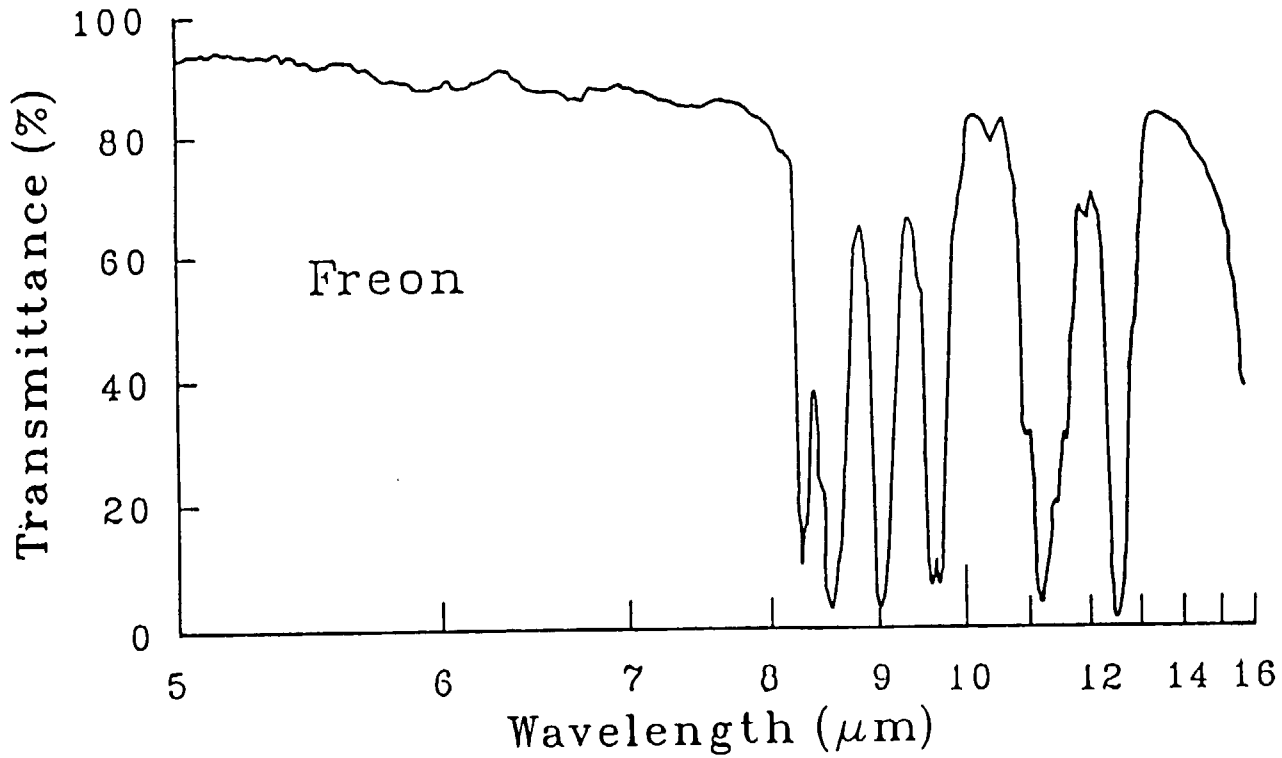

Figure 9. Absorption spectrum for Freon smear reproduced from Reference 15.

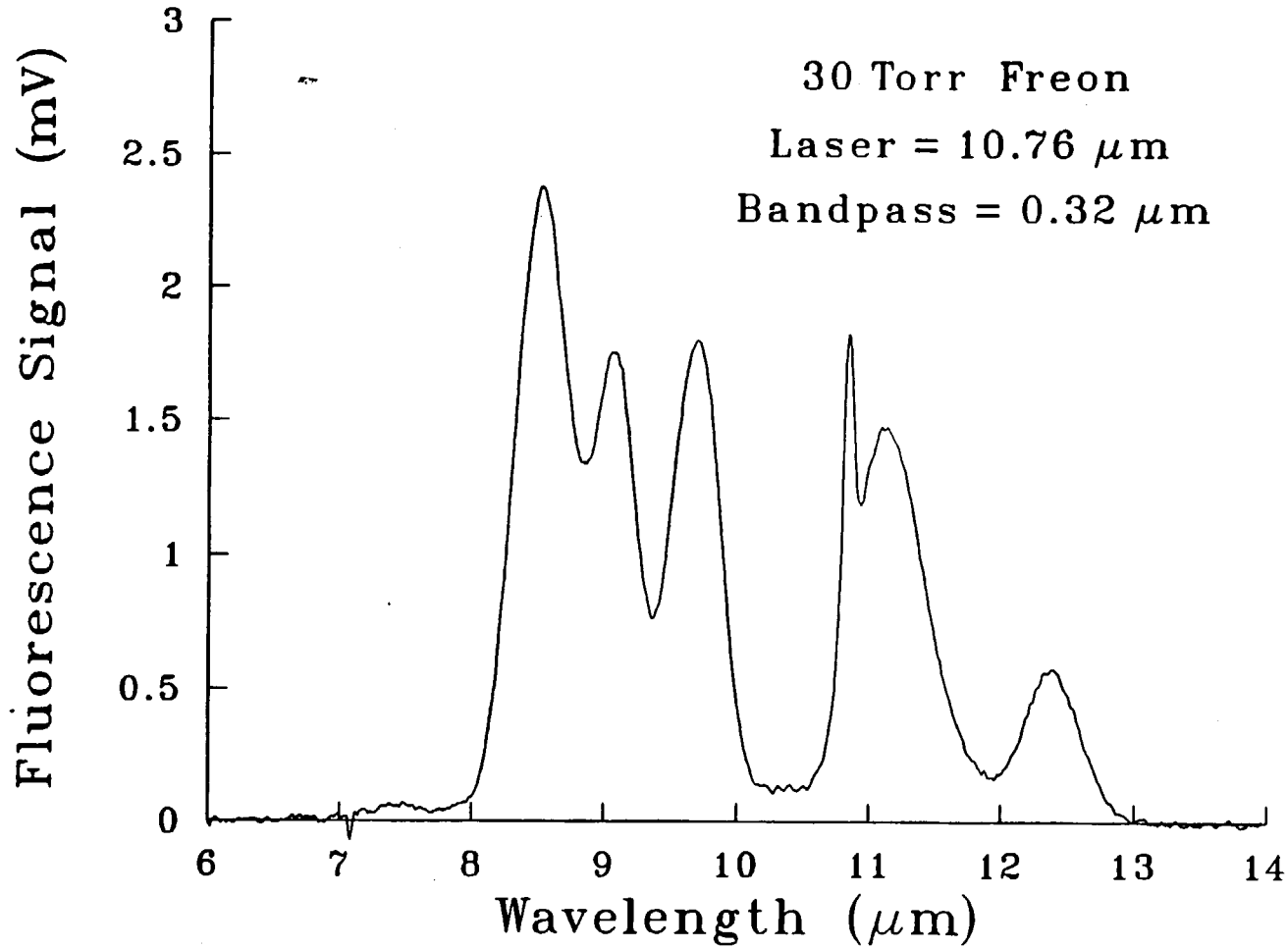

Figure 10. Raw (uncorrected) fluorescence spectra for 30 Torr Freon vapor illuminated with 1.83 W at a laser wavelength of 10.76 μm. The monochromator bandpass was 0.32 μm, and the chamber temperature was 323°K.

described in Section 2.2. Results of these corrections are shown in Figure 11. In the corrected case, the peak heights as well as the peak locations correspond closely to those in the absorption spectrum.

When 7 Torr of Freon vapor was excited by 9.62-μm laser light, the corrected IRF spectrum displayed in Figure 12 was obtained. At this excitation wavelength and vapor pressure, the larger absorption coefficient of Freon greatly reduces the amount of scattered laser radiation. This results in the disappearance of the out-of-phase signal component responsible for the "spikes" occurring at the exciting wavelengths in the spectra shown in Figures 10 and 11. Figure 13 is an IRF spectrum taken under the same conditions as Figure 12 except that the slits were narrowed to give a 0.12-μm bandpass. The three fluorescence peaks between 8 and 10 μm have narrowed, but not to the extent that the "doublet" 8.5-μm peak (see Figure 9) is resolved. Note, however, that while the longer wavelength peaks narrowed, the peaks at 11.3 and 12.3 μm have remained approximately the same width. This can be attributed to the nature of the spectral regions in question. Looking at the absorption spectrum (see Figure 9), the 8- to 10-μm region contains several narrow peaks whose width is considerably less than the monochromator bandpass. The apparent widths of these peaks in the IRF spectrum are a result of the instrumental resolution. The 10- to 12-μm region of the absorption spectrum shows one intrinsically broad absorption peak whose width is already close to or larger than the monochromator bandpass. If the IRF peaks follow the absorption data, this peak can never be narrowed by improving the monochromator's resolution. A program which integrates areas under the spectral radiance curves was run for the 8- to 10.5-μm region of both the wide and narrowed bandpass (0.32 and 0.12 μm) IRF plots of Figures 12 and 13. The resultant IRF radiance (milliwatts/steradian - cubic centimeters) values from each curve agree within two percent. This result indicates that data taken at the wide open slit settings will be sufficient for use in the modeling of the IRF-based remote sensing instrument.

4.2 DMMP (Dimethyl-Methyl-Phosphonate, $(CH_3O)_2$ PO CH_3). The chemical DMMP (a flame retardant chemical additive) has an IR absorption spectrum very similar to the G and V agents and is one of the standard simulants used by investigators who are concerned with chemical agent detection. The IR transmittance versus wavelength spectrum for DMMP is shown in Figure 14.[16] Absorption peaks occur at 7.9 (double), 9.6, 11, and 12.4 μm. Figure 15 depicts a corrected IRF spectrum for 13 Torr DMMP excited with 10.76 μm laser light. A correspondence between the peaks in the absorption and fluorescence spectra in DMMP is again seen with the 7.9-μm double peak being unresolved at this bandpass.

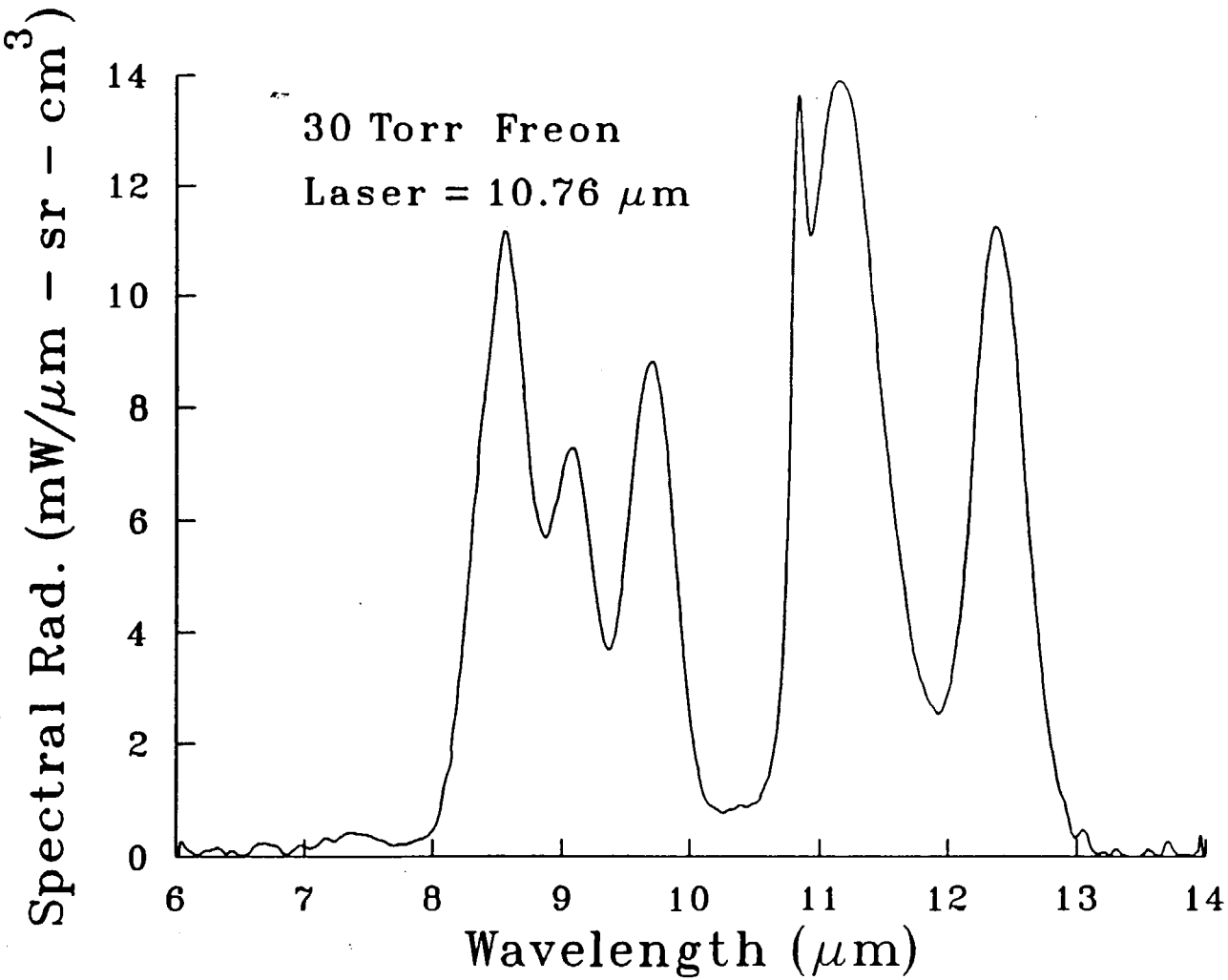

Figure 11. Data from Figure 10 corrected to give the spectral radiance of the 30 Torr Freon vapor for the 1.83 W input power at 10.76 μm.

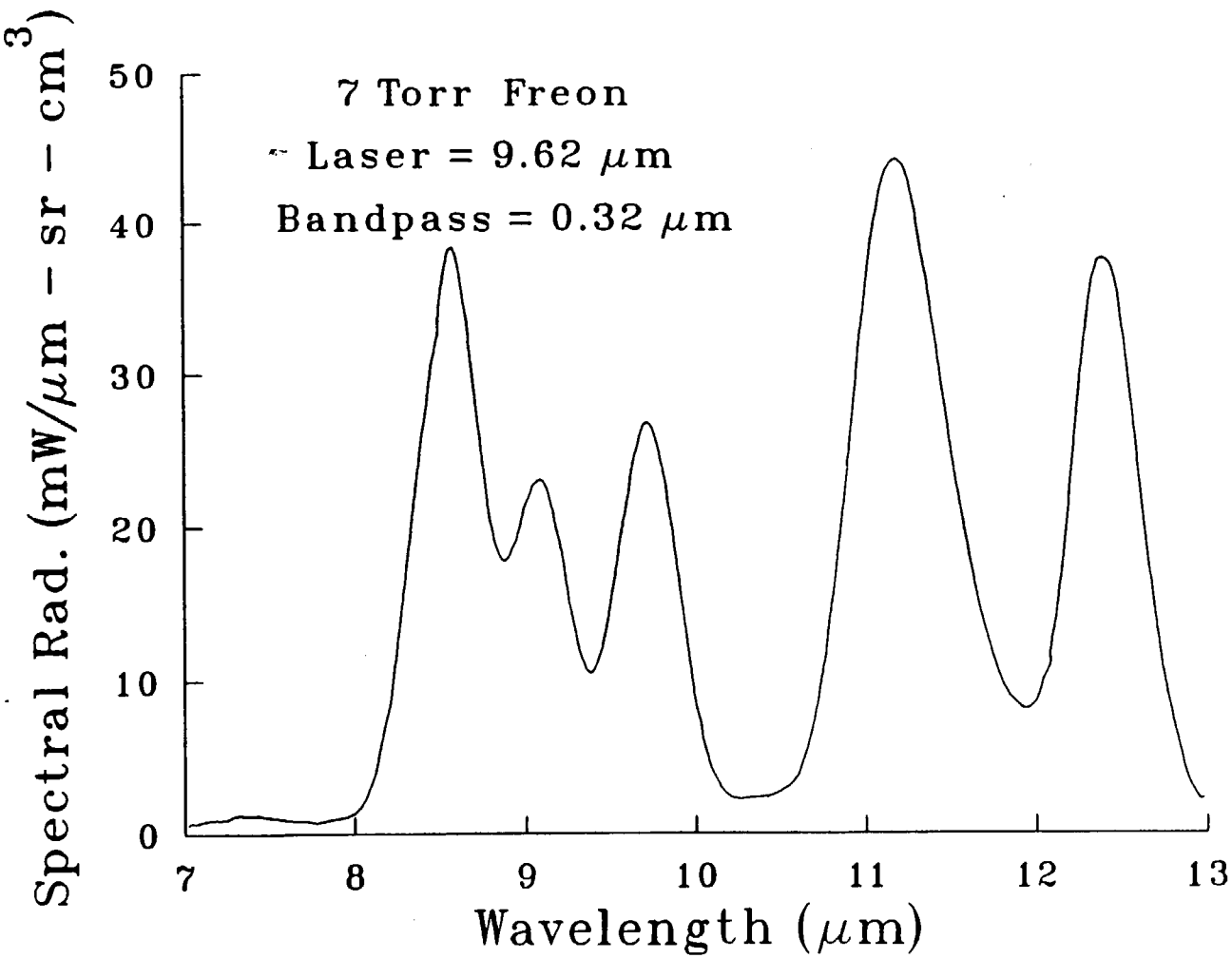

Figure 12. The spectral radiance of 7 Torr Freon vapor illuminated with a 1.85 W laser beam at 9.62 μm. The chamber temperature was 333°K, and the monochromator bandpass was 0.32 μm.

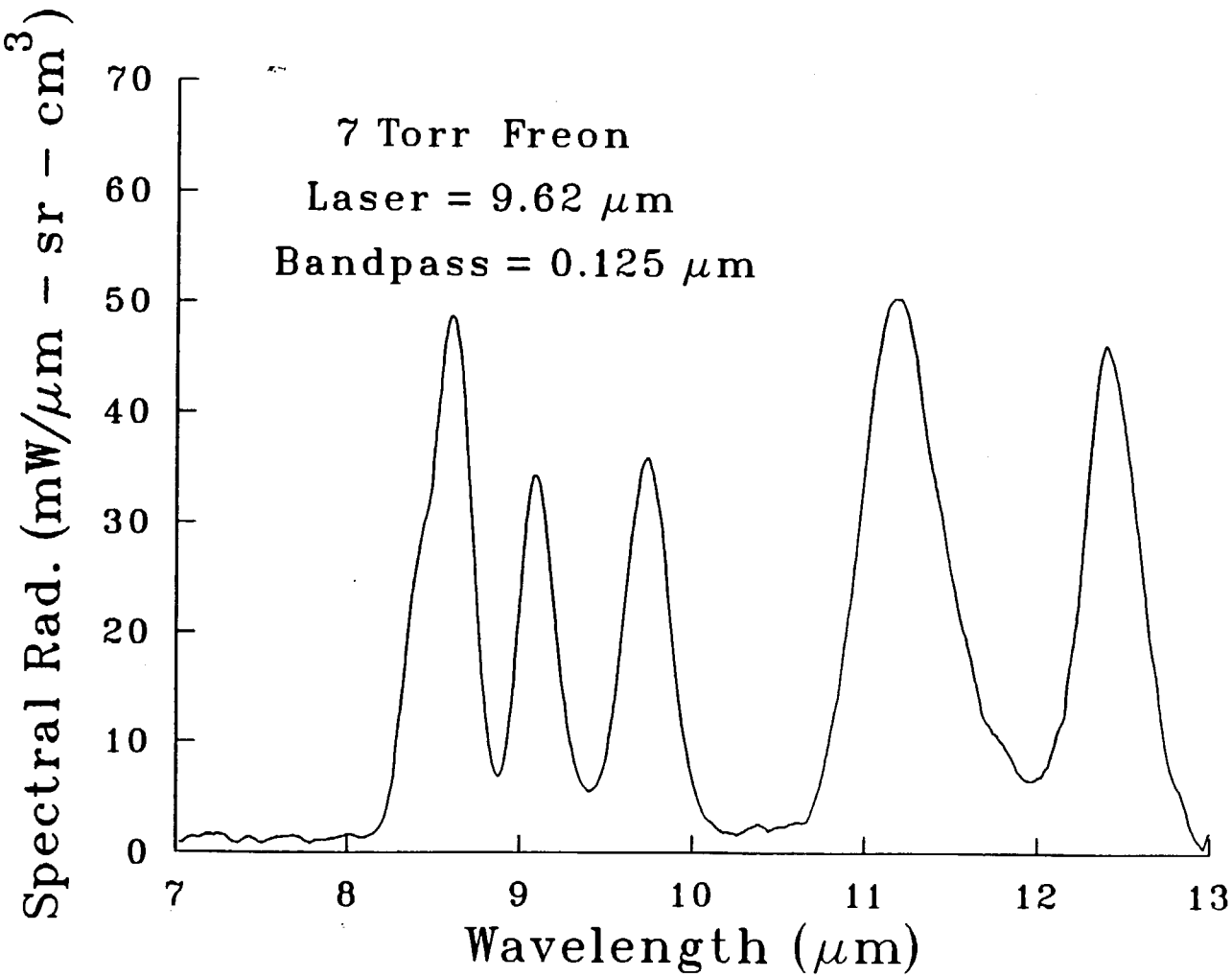

Figure 13. The spectral radiance of 7 Torr Freon vapor illuminated with a 1.85 W laser beam at 9.62 μm. The monochromator bandpass was narrowed to 0.12 μm, and the chamber temperature was 333°K.

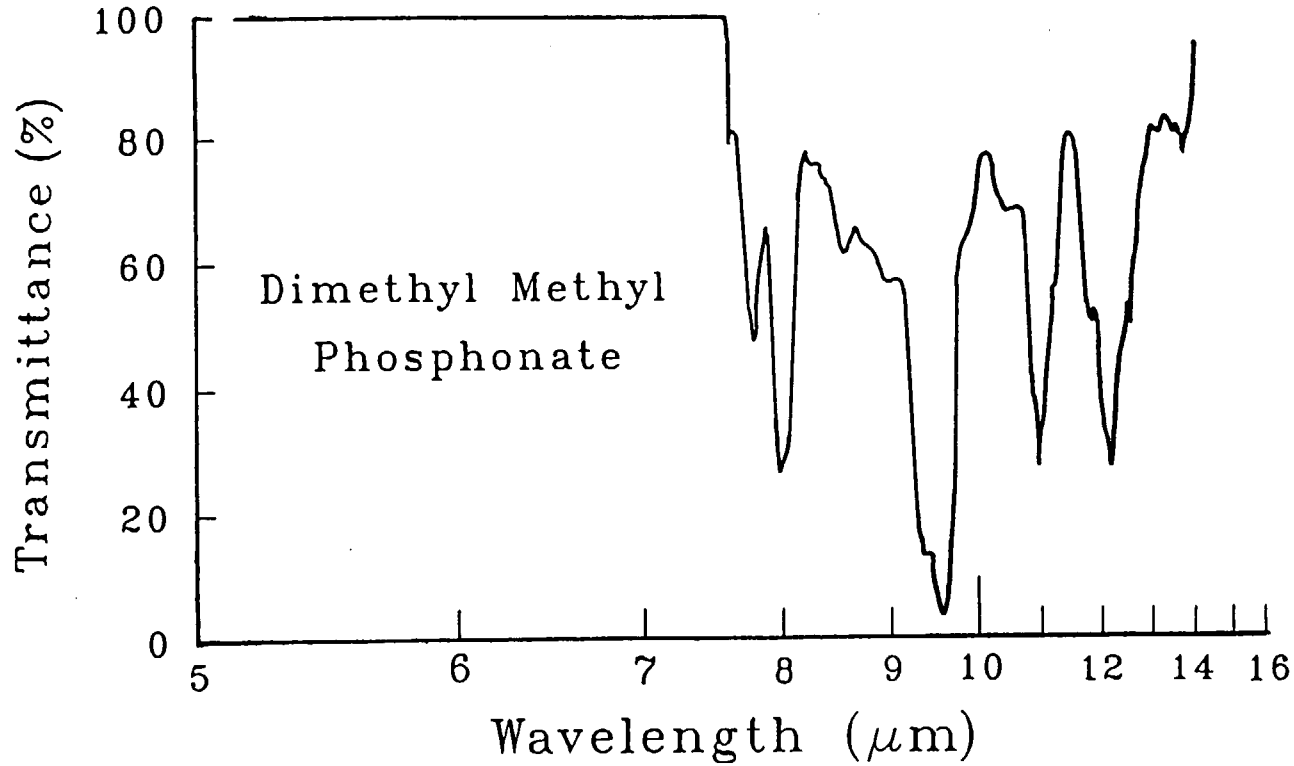

Figure 14. The infrared transmittance of DMMP vapor from 6 to 15 μm from Reference 16. The curve was calculated from measured absorptivities at a concentration-length product of 2,000 mg/m^2.

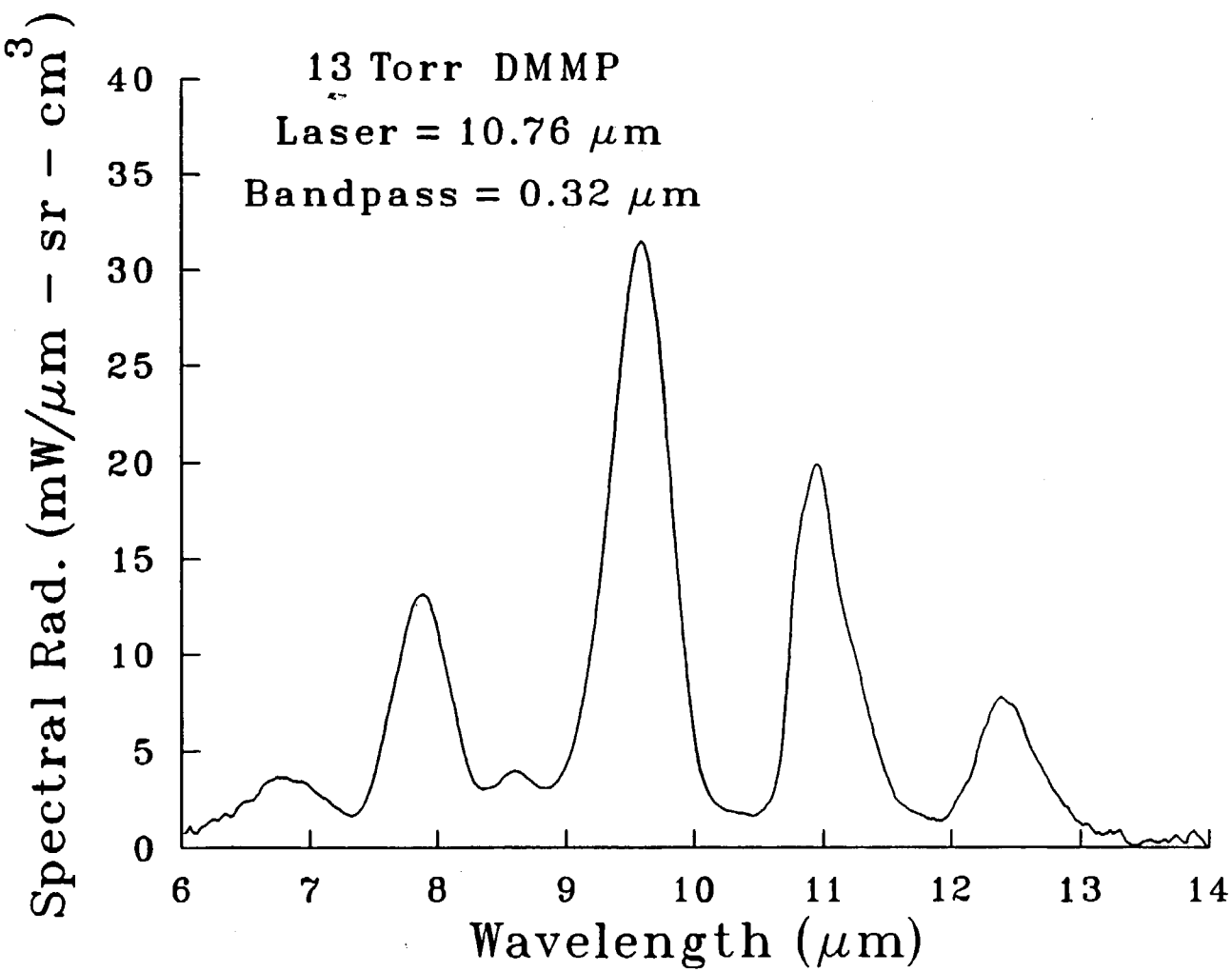

Figure 15. The spectral radiance of 13 Torr DMMP vapor illuminated with 1.8 W at a wavelength of 10.76 μm. The bandpass was 0.32 μm and the chamber temperature was 356°K.

Figure 16 shows a corrected IRF spectrum obtained for a much lower simulant pressure, 3 Torr of DMMP. For this case, the vapor was illuminated with a 9.62-μm beam chopped at 40 Hz. Note, in this case, the signal from IRF transitions near the laser line (corresponding to the large absorption peak) are very large and are greater than the full-scale response of the lock-in amplifier.

4.3 Ethylene. Ethylene, a gas with an IRF spectrum typical of many substances found in internal combustion engine exhausts, has been studied previously by Robinson, et al.[17,18] In the latter study the investigators used a 30-W cw CO_2 laser operating at 10.6 μm and chopped at 10 Hz to illuminate the ethylene gas. The emitted fluorescence was sensed with a modified Beckman model IR-10 spectrometer that was equipped with a thermocouple detector. In the present work, we report measurements of ethylene's IRF spectra, which, because the apparatus possesses an improved collection/detection efficiency and has been calibrated against a source of known radiance, feature not only signal-to-noise ratios higher than prior work but also quantitative spectral radiances. The general features of the spectra, however, are in good agreement with those of Robinson and his colleagues.

The results obtained when 100 Torr of ethylene at room temperature (283°K) was excited by a 2.65-W, 10.6-μm beam chopped at 10 Hz are illustrated in Figure 17. A peak at 7 μm and a broad peak centered at 10.5 μm appear. Uncorrected spectral scans from 4 to 14 μm reveal a third fluorescence peak centered at 5.3 μm.

4.4 Methyl Alcohol. Methanol is another previously studied, easily vaporized liquid whose IRF spectra were obtained. The methanol absorption spectrum exhibits two broad peaks, one at 7 μm and a larger peak centered at 9.8 μm. The corrected fluorescence spectrum for 103 Torr methanol excited at 10.27 μm is shown in Figure 18. As in the case of ethylene, Robinson and Katayama have also acquired low signal-to-noise ratio IRF spectra of methyl alcohol.[18] The present work agrees well with that of our predecessors and shows a strong correlation with the IR absorption spectrum of this chemical.

Having surveyed the IRF spectra in the preceding cases and those previously measured by Robinson and his coworkers (which, taken together, are considered to represent the typical chemical compositions/structures of potential military target aerosols),[7] we decided to concentrate our further studies on two materials, Freon and DMMP. The selection of these two agent simulants was based upon two primarily practical considerations. First, both are pure, nonflammable substances with a relatively clean chemistry that renders their fluorescence properties more suitable for modeling and field testing. Second, we noted that the concentrations of interest in threat agent sensing are generally lower than those required for exhaust detection. A system which can be built for attacking the agent

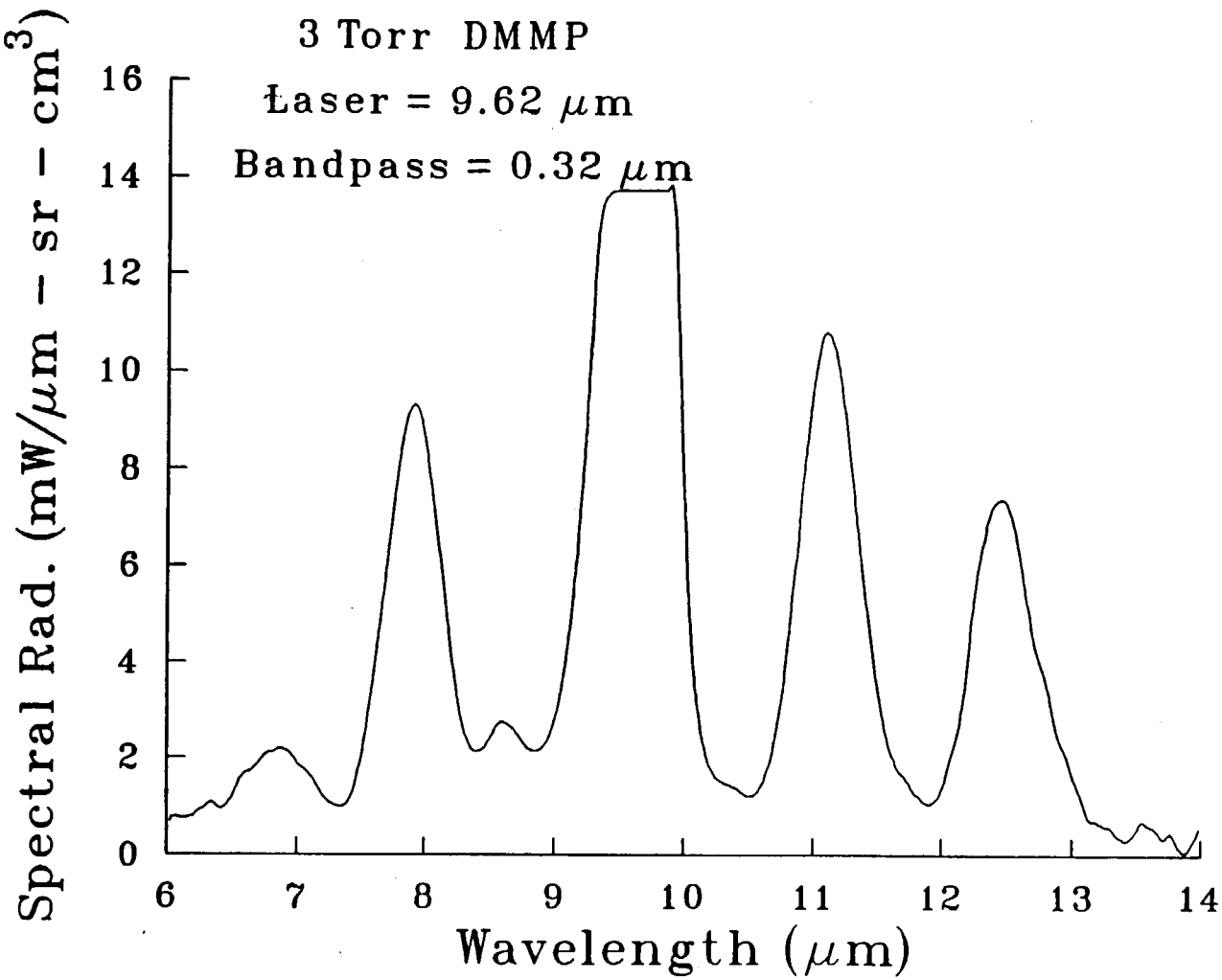

Figure 16. The spectral radiance of 3 Torr of DMMP vapor illuminated with a 1.75 W laser beam at 9.62 μm. The bandpass was 0.32 μm with a chamber temperature of 353°K.

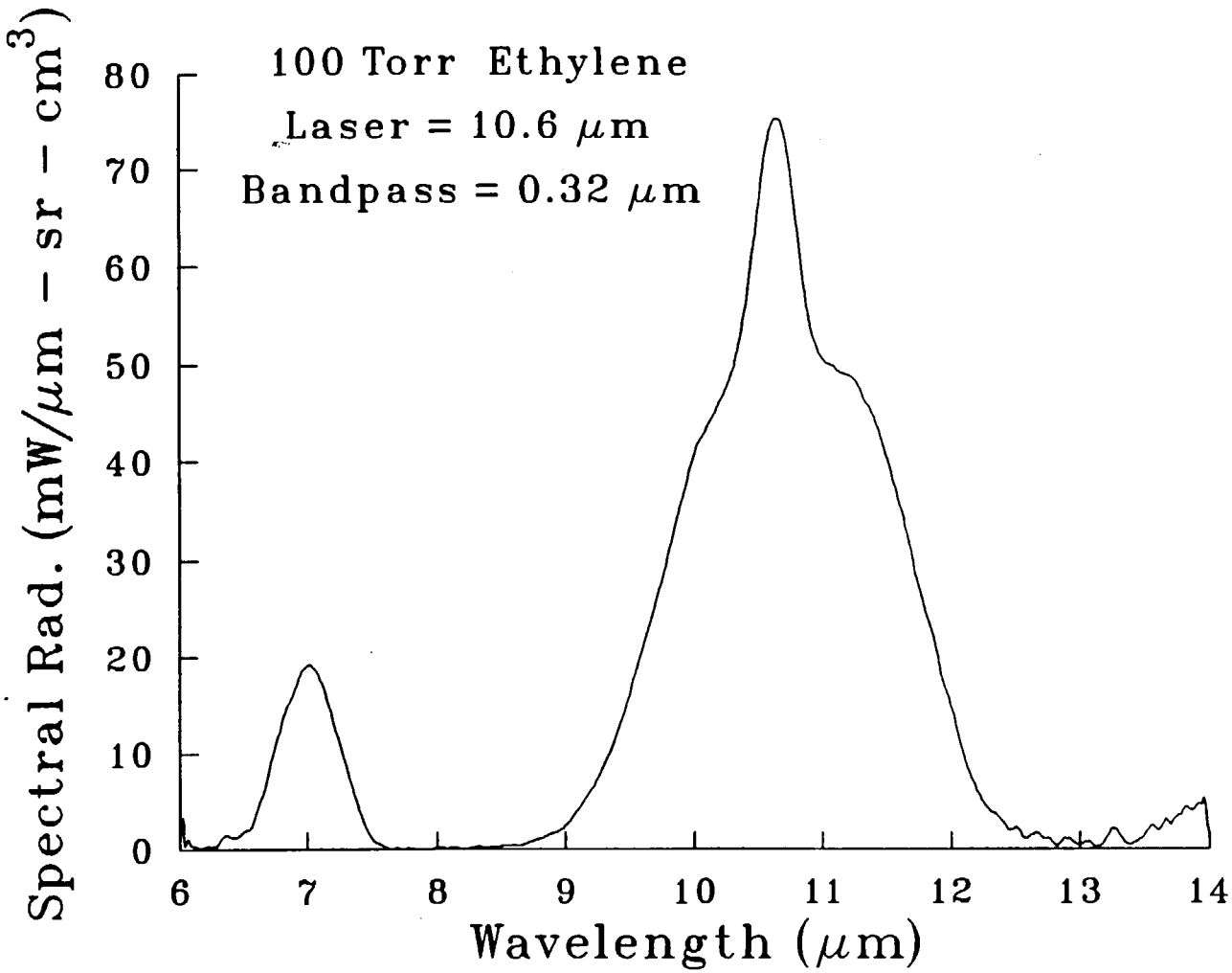

Figure 17. The spectral radiance of 100 Torr of ethylene gas excited at 10.6 μm with a 2.65 W laser beam. The bandpass was 0.32 μm, and the chamber was at room temperature.

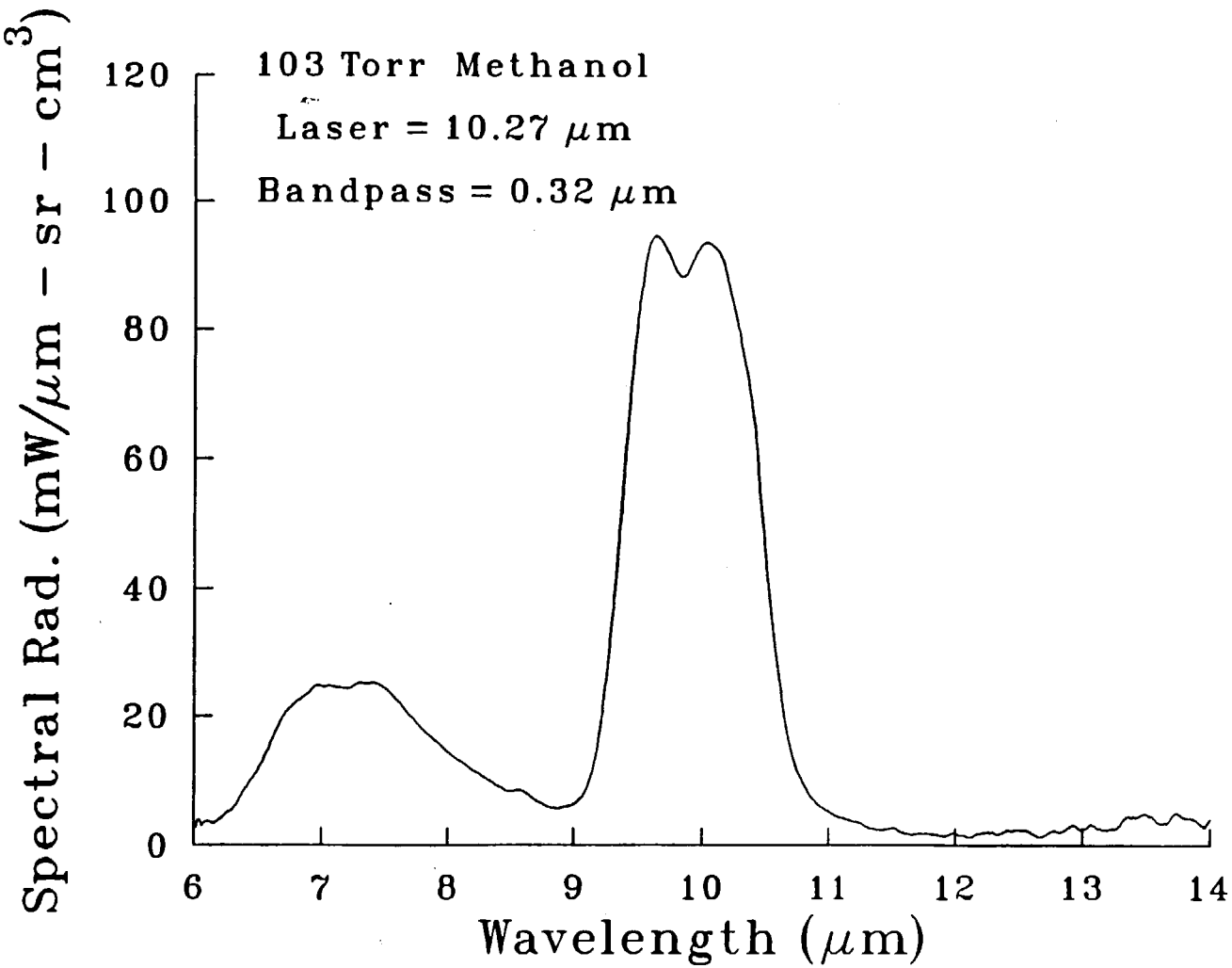

Figure 18. The spectral radiance of 103 Torr methyl alcohol vapor illuminated with 2.8 W at a wavelength of 10.27 μm. The bandpass was 0.32 μm, and the chamber temperature was 328°K.

problem would also certainly satisfy many requirements in the exhaust, environmental and process control arenas.

Accordingly, the remaining portions of this report and the subsequent report on the modeling of remote sensing schemes will concentrate on Freon and DMMP.

4.5 Spectra at Atmospheric Pressure. The ultimate factor which will determine if IRF has potential for the remote sensing of agents and exhausts is whether or not enough fluorescence is induced to render the vapor detectable, especially when dispersed in the atmosphere. We, therefore, acquired spectra of Freon-air and DMMP-air mixtures in order to quantitatively assess the amount of fluorescence surviving atmospheric quenching and to determine if any other properties of their IRF signals differed from those found with the pure vapors.

Figure 19 shows the typical effect of quenching. The IR fluorescence it depicts (dashed curve) comes from a Freon-air mixture at one atm. The partial pressure of Freon in the mixture is 30 torr, and the illuminating laser was tuned to 10.76 μm. Note that except for the addition of the air, the conditions prevailing in Figure 19 are the same as those in Figures 10 and 11. A comparison of the respective 8.6-μm peak heights indicates that approximately 8.7 percent of the fluorescence signal remains after the addition of air. This percentage is a significantly more residual signal than expected from extrapolations based upon the vibrational and fluorescence lifetimes of molecules like CO[6]. It is similar to results for 35 Torr ethylene in air obtained by Robinson and Dake,[7] who observed that 14 percent of the fluorescence signal between wavelengths of 7 and 14 μm (for 10.6-μm illumination) survived after the addition of air to one atm. Our interpretation of this promising result will be offered in the next section.

A similar effect is observed in DMMP. The spectrum for 13 Torr DMMP, taken under the same conditions as those in Figure 14 except for the addition of air to one atm, is shown in Figure 20. In this case, a comparison of the 9.6-μm peak heights indicates approximately 9.5 percent of the fluorescence is still present after the addition of air--again, significant IRF stays unquenched for the excitation wavelength of 10.76 μm for the DMMP vapor-air mixture. Vapor-air mixtures of either Freon or DMMP when excited with 9.6-μm laser light were found to exhibit larger quenching of the IR fluorescence signal. In these cases, good signal-to-noise ratio spectra were more difficult to obtain.

4.6 Chopping Period Versus Fluorescence Output. A systematic study of the effect of independently varying each of the several experimental parameters governing fluorescence turned up one particularly notable and revealing phenomena. This came when the simulant vapor pressure, laser

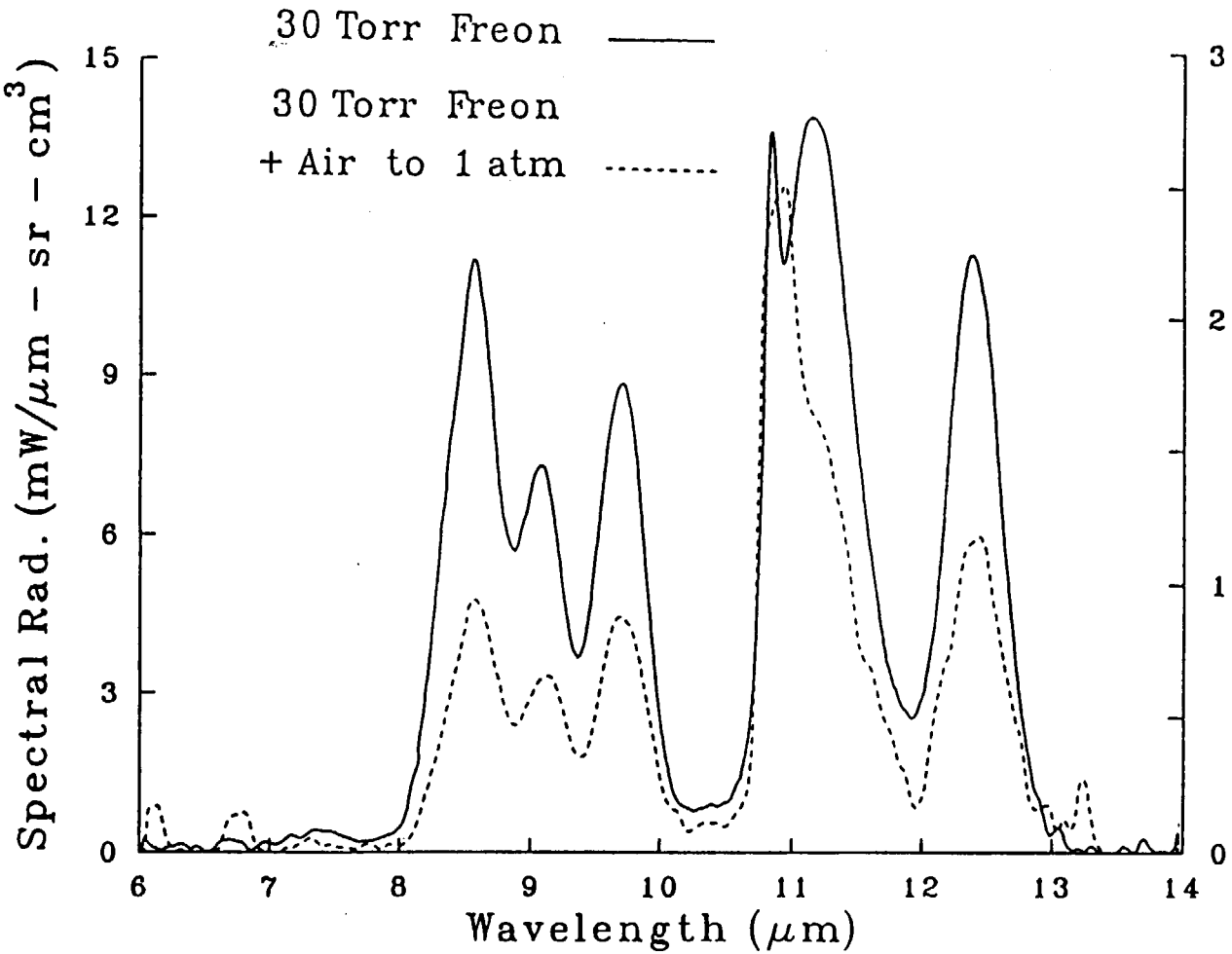

Figure 19. The spectral radiance of a mixture of 30 Torr Freon plus air added to 1 atm (dashed curve - right vertical scale). The data were taken under the same conditions as Figures 10, 11 and are compared to that for a pure Freon vapor at 30 Torr (solid curve - left vertical scale).

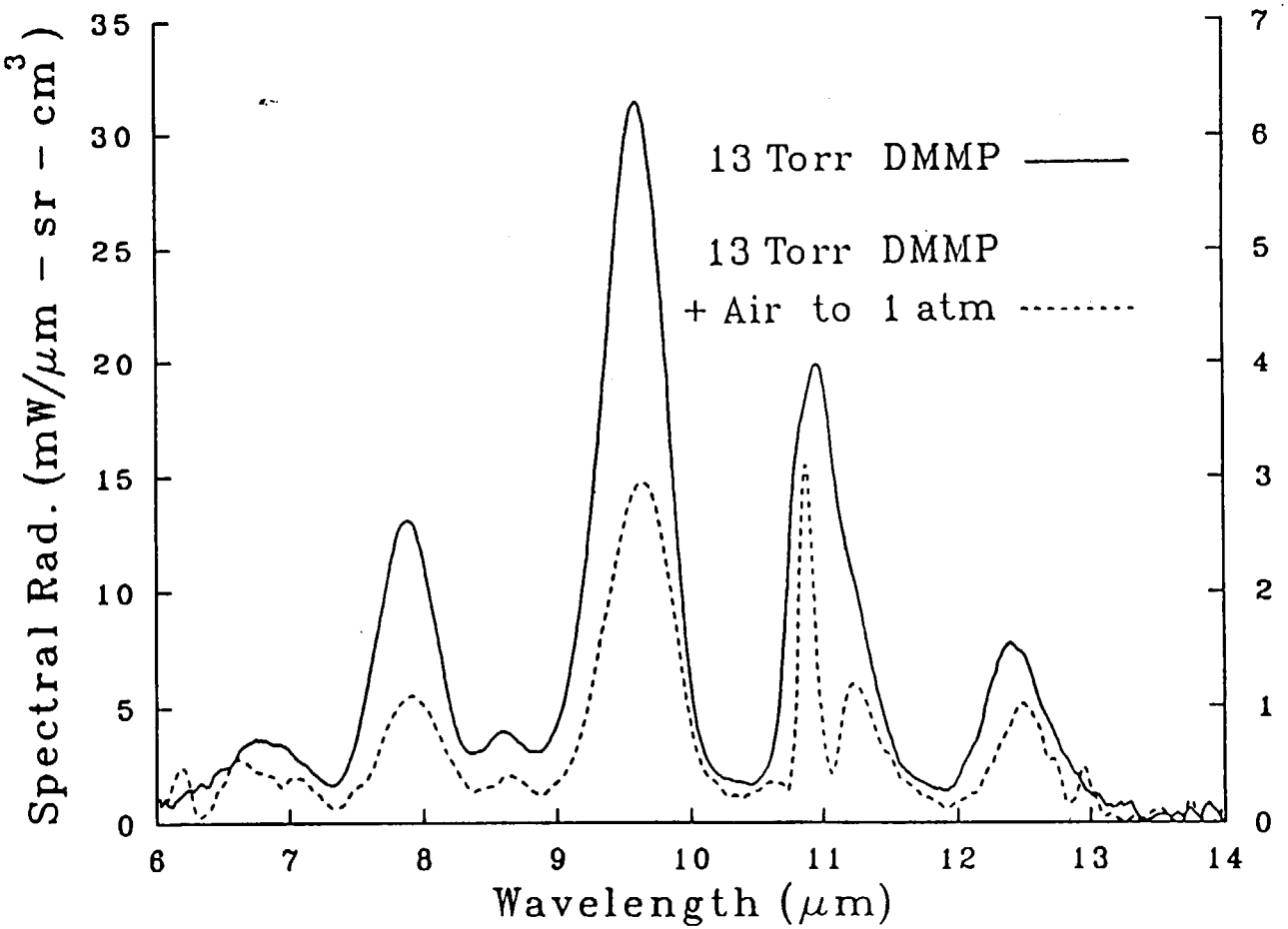

Figure 20. The spectral radiance of a mixture of 13 Torr DMMP plus air added to 1 atm (dashed curve - right vertical scale). The data were taken under the same conditions as Figure 15 and are compared to that for a pure DMMP vapor at 13 Torr (solid curve - left vertical scale).

wavelength/power and fluorescent wavelength were all held fixed and the chopping frequency was altered. The IRF signal intensity was found to vary linearly with the illumination period (1/chopping frequency) for all but the lowest pressures (< 5 Torr) of simulant vapor. When the simulant pressure was small, some saturation of the signal was observed for large values of chopping period, causing the signal intensity to begin to flatten towards some maximum value.

Two figures illustrate these effects. Figure 21 plots the raw fluorescence intensity monitored at 8 μm versus chopping period for 10 Torr of Freon excited at a wavelength of 9.63 μm. A linear relationship is observed out to 100 msec. Conversely, for lower pressures of Freon vapor (1 Torr--see Figure 22), saturation has caused the fluorescence signal to exhibit nonlinear behavior at larger values of chopping period (> 20 msec). In both measurements, the grating monochromator was replaced with an IR interference filter whose passband was 7.5-8.5 μm. Figure 23 shows similar saturation at the longer chopping periods takes place at other exciting wavelengths. It shows the raw, 8-μm wavelength IRF signal coming from 1 Torr of Freon when excited at 10.76 μm. However, we found that if air was added to these small quantities of vapor until the mixture reached atmospheric pressure, the IRF signal remained unsaturated even out to 200 msec chopping periods (the bandwidth limit of our amplifiers). The absence of saturation also may be seen in the data of Figure 24. Here the IRF intensity versus chopping period is plotted for 1 Torr of Freon excited at 10.76 μm just as in Figure 23, but this time air was added to produce one atm total pressure.

Similar behavior was observed in the IRF signal intensity from a mixture of air and another vapor, DMMP (14 Torr DMMP plus air to one atm mixture). In this case, fluorescence was detected at 9.5 μm (0.32-μm bandpass) as seen in Figure 25, where its intensity is plotted as a function of the chopping period. The laser excitation wavelength was 10.76 μm, and the power into the chamber was 1.75 W. Here, as well, a linear increase of the fluorescence signal is observed out to long (100 msec), laser-chopping periods with no evidence of saturation appearing in the period dependance. Assuming that the same linear time/fluorescence intensity behavior observed in the IRF signals emanating from the vapor-air mixtures studied here is widespread, the modeling of the performance of remote sensing systems operating at different laser pulse-chopping rates will be simplified.

5. DISCUSSION OF RESULTS AND CONCLUSIONS

As a starting point, it is instructive to compare the absorption spectra of the complex molecules studied here (Figure 9, 14) with the well-known absorption features of simpler polyatomic molecules (CO, CO_2, for example).[6] None of the regularly spaced, easily distinguished, vibro-rotational fine structure evident in the latter is observed. This can be attributed to the reduced vibro-rotational

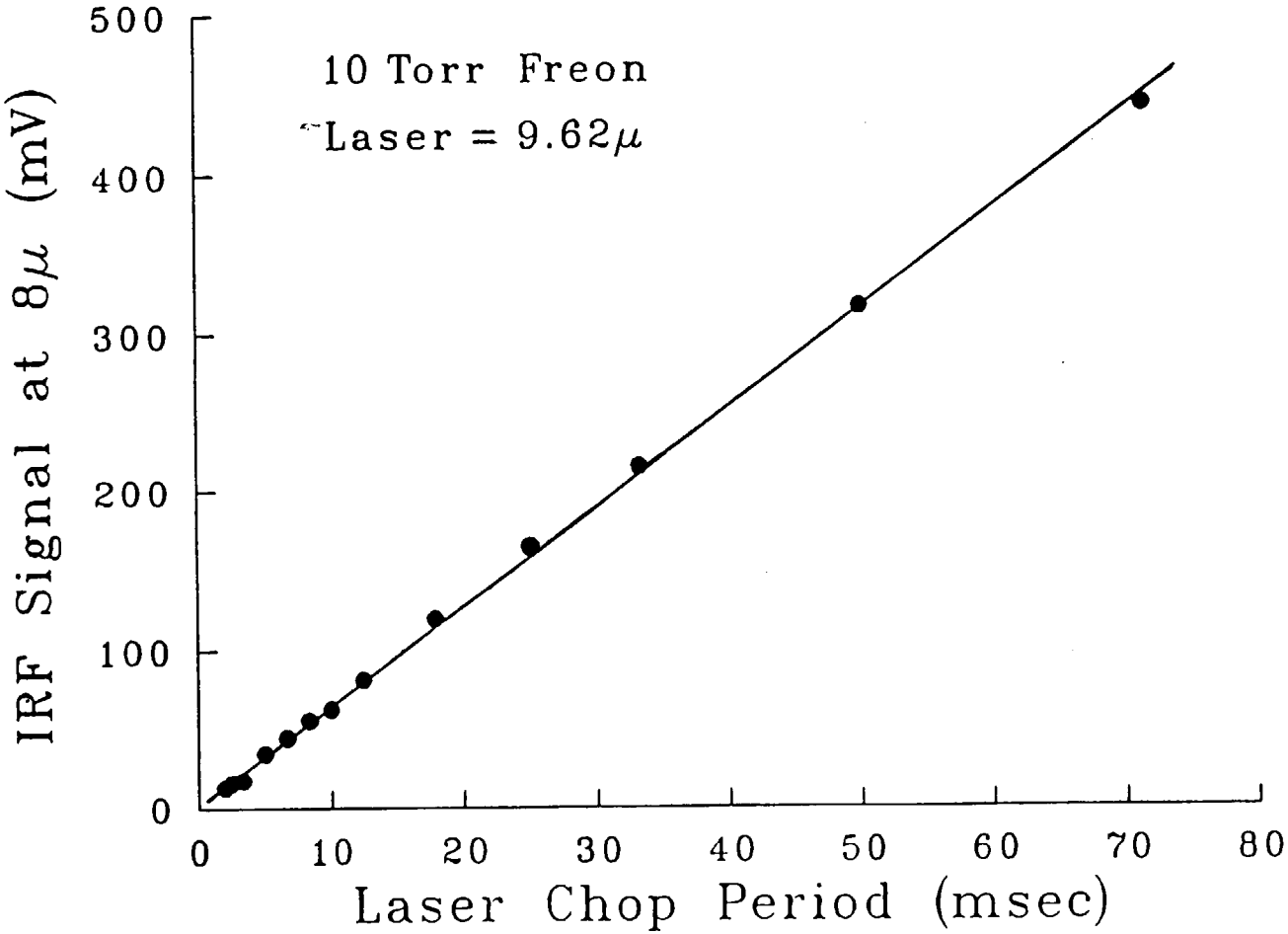

Figure 21. Fluorescence intensity through 8 μm filter (1 μm bandpass) versus laser chopping period for 1 Torr Freon vapor excited at 9.63 μm and 1.28 W of laser power. Chamber temperature was 326°K.

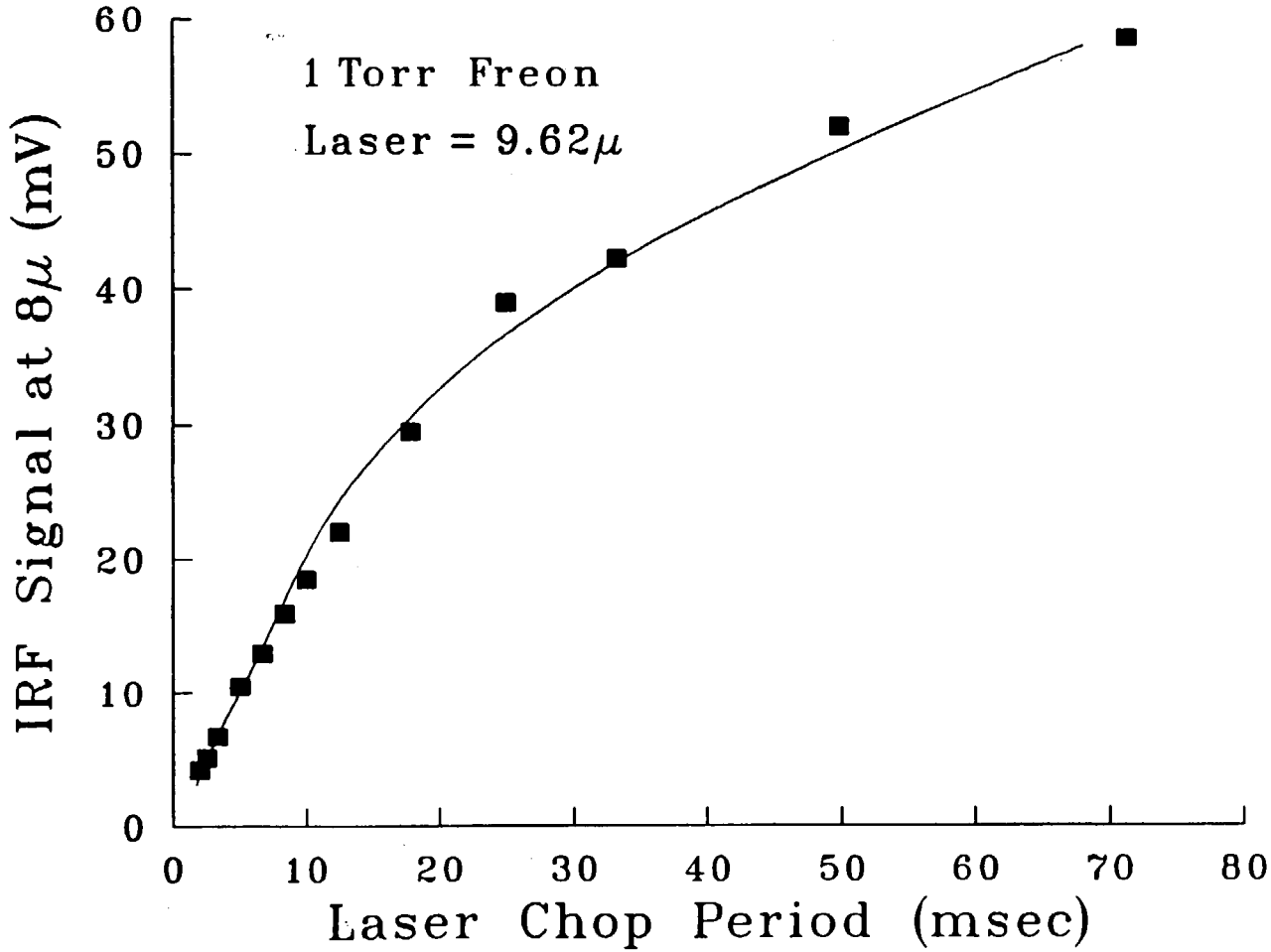

Figure 22. Fluorescence intensity through 8 μm filter (1 μm bandpass) versus laser chopping period for 1 Torr Freon vapor excited at 9.62 μm and 1.3 W of laser power. Chamber temperature was 326°K.

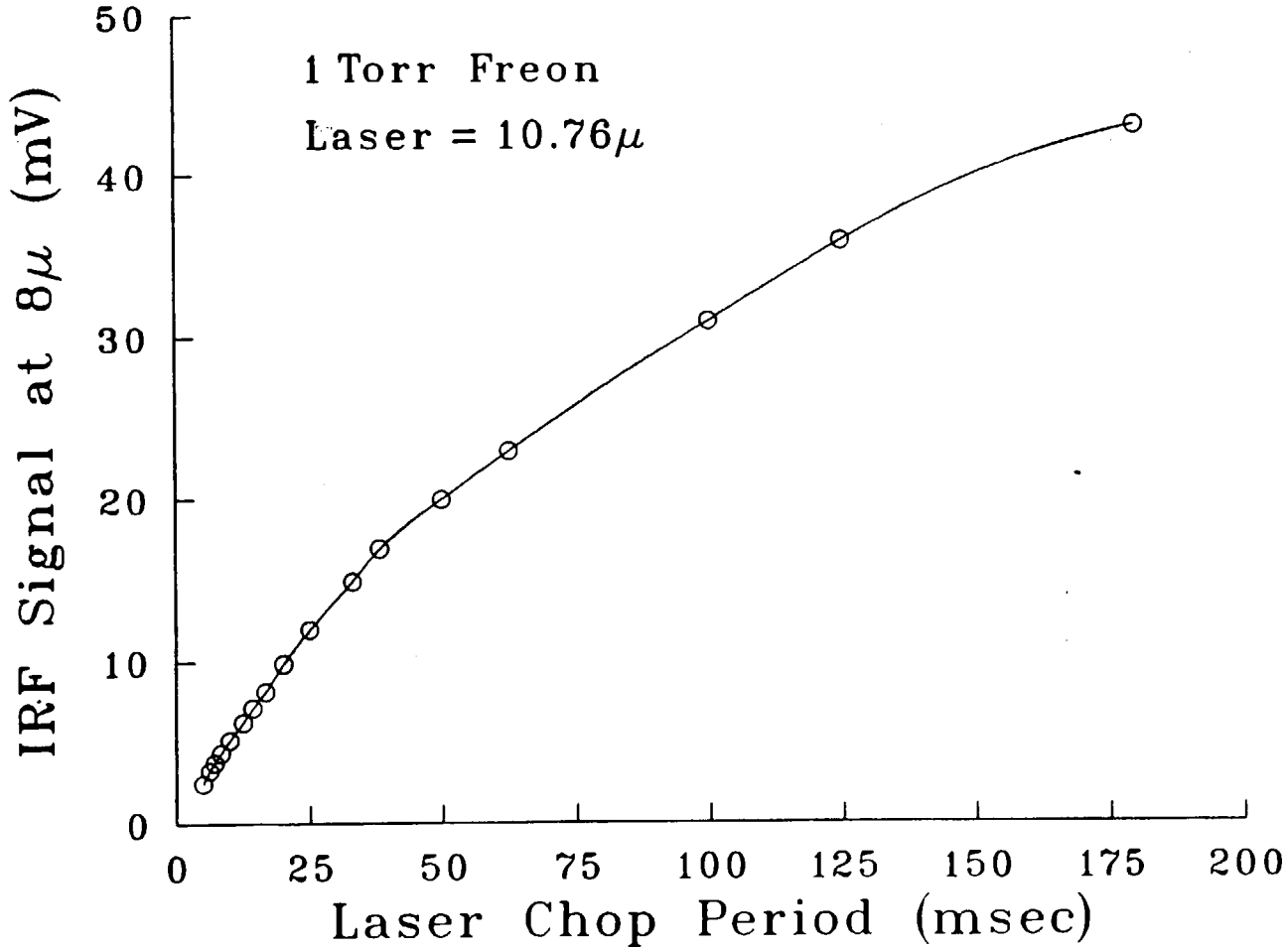

Figure 23. Fluorescence intensity through 8 μm filter (1 μm bandpass) versus laser chopping period for 1 Torr Freon illuminated at 10.76 μm with 1.7 W laser power. Chamber temperature was 328°K.

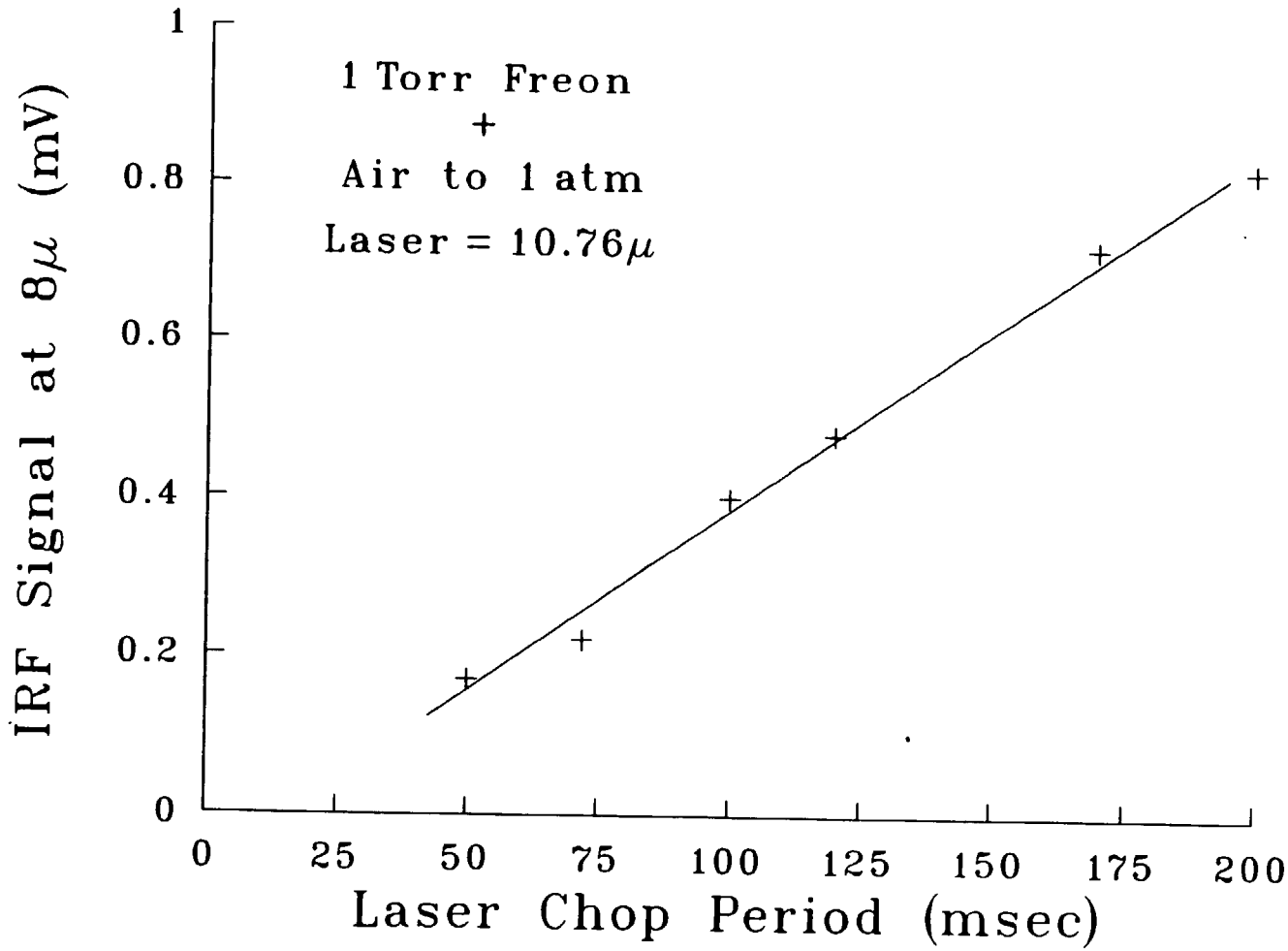

Figure 24. Fluorescence intensity through 8 μm filter (1 μm bandpass) versus laser chopping period for same 1 Torr Freon as Figure 23 only with air added to 1 atm total pressure. The mixture was illuminated with the laser at 10.76 μm and 1.7 W laser power. The chamber temperature was 328°K.

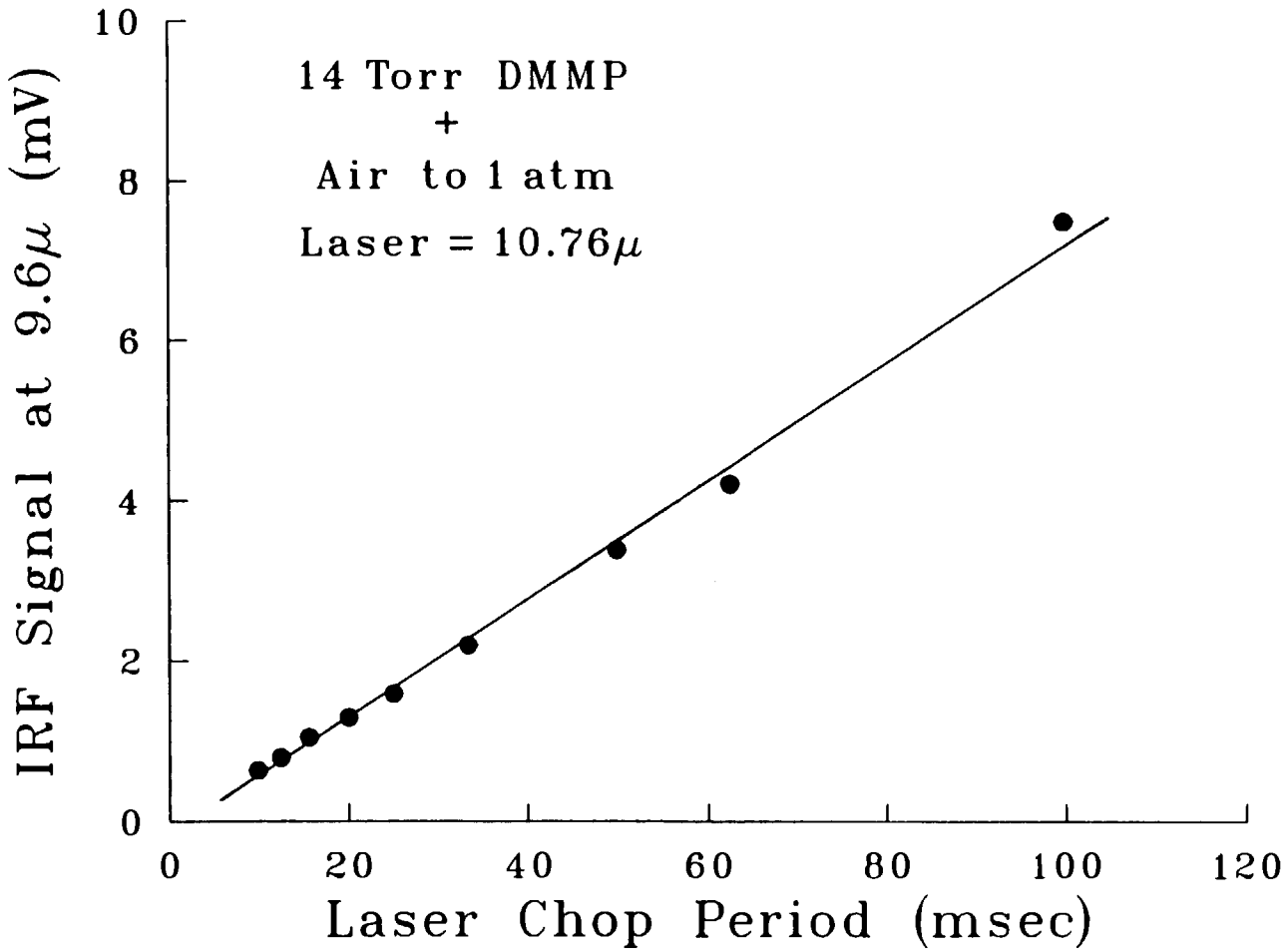

Figure 25. Fluorescence intensity through the monochromator at 9.6 μm (0.32 μm bandpass) versus laser chopping period for 14 Torr DMMP with air added to 1 atm total pressure. The mixture was illuminated at a wavelength of 10.76 μm with 1.45 W of laser power. The chamber temperature was 353°K.

line spacing characteristic of large molecules, and the random line positioning that results from their overall structural asymmetry. Together, these effects cause the individual lines to coalesce to an extent that they are rarely resolved. No fine structure has been observed in G and V agents vapor IR absorption spectra even at low pressures and high instrumental resolutions.[16]

Examining the actual features in the present IRF data, one notices that they seem to reflect overall structural similarity with the absorption results. From this similarity, we infer that if a vapor is excited at one of its resonant absorption lines, the energy acquired by the molecule is rapidly redistributed among the other vibro-rotational modes of the molecule via intramolecular (mode-mixing) means. Almost immediately collisional processes redistribute the energy to other vapor molecules and, if the target is a mixture, to the surrounding air. Molecules in this locally heated region manifest their excess energy in several ways--energy transfer to the surrounding aerosol, nonradiative redistribution to other vibro-rotational modes, and IR radiation. The last process produces the fluorescence emission upon which this work is based. The principle of detailed balance leads one to expect that radiation will take place at favored IR transition wavelengths--in other words, at the same wavelengths at which resonant absorption occurs. The end result is that the IRF spectra should mimic the IR absorption spectra of the participating molecules--precisely the situation found by Robinson, his co-workers, and by us. On a practical note, this behavior is very important, for it means that the wavelength dependence of fluorescent emission can be used as a fingerprint for identification in remote sensing, and, furthermore, that fingerprint should be very similar to the often-catalogued absorption spectra.

Other conclusions about the nature of the fluorescence process can be derived from looking at the IRF signal waveform and the chop frequency versus IRF signal data. Our observation of the IRF signal's waveform shows slow rise and decay times (> 1 msec) for slowly chopped (< 1kHz) laser excitation. This observation suggests that the fluorescence is strongly tied to the bulk heating of the vapor or vapor-air mixture along the beam path. Such results were predicted and observed by Bailey and Cruickshank.[11] The conclusions as to their nature are strongly reinforced by the linear dependance of the IRF intensity with laser illumination period. To understand the origin of this relationship, one should consider a chopped laser beam that is heating an absorbing vapor. If the vapor takes a time period much longer than the chop pulse width to reach thermal equilibrium, the vapor temperature will increase during the illumination portion of the waveform and decrease during the nonilluminated portion as each pulse is received. The temperature rise will exceed the fall until the vapor-air mixture reaches a temperature gradient with the surrounding gas sufficient to cause the conduction and radiation losses during the entire pulse period to equal that coming in during illumination. Because the gas in the laser beam column is brought to a temperature higher than the surrounding gas, it will emit IR in a near-continuous fashion. This DC emission will not be directly observed in our apparatus because our

detection electronics are AC coupled. However, during each chop cycle the laser beam will modulate the column temperature slightly; it will rise during illumination and will cool during the portion in which the beam is blanked off. The extent of this temperature excursion depends on the length of time the target is illuminated during each cycle and the length of time it has to cool--that is, the illumination period. If the period is long, the gas will have a chance to warm considerably before the beam is chopped off and, conversely, to cool extensively before it comes back on. Given that the amount of IRF is proportional to the number of excited molecules, which, in turn, can be related to the vapor's temperature, it is not surprising that the size of the signal produced by an AC coupled detector will appear to grow as the period is lengthened.

Further support of the picture of a fluorescence process dominated by thermalizing is the fact that vapor-air mixtures are not quenched to the extent expected by fluorescence and vibrational lifetime estimates that come out of short-pulsed laser work. Under this type of illumination and with vibrational radiative lifetimes in the msec range, the much faster (μsec) collisional processes in an air-vapor mixture will quickly quench the fluorescence from the excited molecules. The behavior witnessed in the present studies indicates thermal conduction and diffusion are governing fluorescent emission and decay by constantly repopulating excited states. The fluorescence lifetimes observed with short-pulse laser excitation clearly are inappropriate descriptors of this regime.

The disappearance of slow chop rate saturation effects when low pressure simulants undergo the addition of air is due to both the increased collisional de-excitation and increased thermal conduction to the surroundings (chamber walls, etc.) at one atm pressure. The fluorescent output is obviously decreased, but quenching leaves plenty of simulant molecules in states that the long period of laser illumination will be able to re-excite. The result is nonsaturated IRF signals from these vapor-air mixtures and linear behavior for even long laser illumination periods.

The finding that the IRF signal intensity depends linearly on the laser illumination period suggests that slowly chopped/pulsed laser excitation may provide sufficient sensitivity for remote sensing using IRF emissions. Although this practically eliminates attaining range resolution from timing the returned signals, other techniques such as triangulation using two separate detectors could compensate for this shortcoming. IRF seems to offer other substantial advantages. A remote sensing system based on fluorescence requires only one CO_2 laser, whose intensity need not be known precisely (unlike DIAL/DISC, wherein two lasers, each at different wavelengths, not only require careful output monitoring, but also retuning for each different substance measured). Beyond being much simpler to design/operate and independent of the reflective albedo of background scenery, the present means has another decided advantage--specifically, the detected fluorescence signals themselves contain the

information needed to identify a threat agent or an active battlefield vehicle. Simple circular, variable filters or high throughput interferometers would be able to scan for and identify these substances at wavelengths differing from that of the laser's, thus minimizing effects of airborne dust and aerosols, which can affect other laser remote sensing techniques.

Results indicate that further work to obtain the data needed for modeling IRF remote sensing is warranted. Such studies are, in fact, currently underway.

INTENTIONALLY LEFT BLANK.

6. REFERENCES

1. Wright, M.L., and G. Gioumousis. "Studies of DIAL/DISC Remote Sensing Techniques for Chemical Agent Detection." ARSCL-CR-80042, U.S. Army Chemical Systems Laboratory, Aberdeen Proving Ground, MD, May 1980.

2. Hirschfield, T., E.R. Schildkraut, H. Tannenbaum, and D. Tannenbaum. "Remote Spectroscopic Analysis of PPM-Level Air Pollutants by Raman Spectroscopy," Applied Physics Letters. Vol. 22, No. 1, p. 38, 1973.

3. Christesen, S.D. "The Application of Stimulated Raman Gain and Inverse Raman Spectroscopy to the Remote Detection of Chemical Agents." CRDEC-TR-87033, U.S. Army Chemical Research, Development, and Engineering Center, Aberdeen Proving Ground, MD, August 1987.

4. Gehlhaar, U., K.P. Gunther, and J. Luther. "Compact and Highly Sensitive Fluorescence Lidar for Oceangraphic Measurements," Applied Optics. Vol. 20, No. 19, p. 331, 1981.

5. Gelbwachs, J. "NO_2 Lidar Comparison: Fluorescence Versus Backscattered Differential Absorption," Applied Optics. Vol. 12, No. 12, p. 2812, 1981.

6. Kildal, H., and R. Byer. "Comparison of Laser Methods for the Remote Detection of Atmospheric Pollutants," Proceedings of the Institute of Electrical and Electronic Engineers. Vol. 59, p. 1644, 1971.

7. Robinson, J.W., and J.D. Dake. "Remote Sensing of Air Pollutants by Laser-Induced Infrared Fluorescence--A Review," Analytica Chimica Acta. Vol. 71, p. 277, 1974.

8. Hocker, L.O., M.A. Kovacs, C.K. Rhodes, G.W. Flynn, and A. Javan. "Vibrational Relaxation Measurements in CO_2 Using an Induced Fluorescence Technique," Physical Review Letters. Vol. 17, No. 5, p. 233, 1966.

9. Bates, R.D., G.W. Flynn, and A.M. Ronn. "Laser-Induced Vibrational Fluorescence in Nitrous Oxide," Journal of Chemical Physics. Vol. 49, p. 1432, 1968.

10. Yardley, J.J., and C.B. Moore. "Vibrational Energy Transfer in Methane," Journal of Chemical Physics. Vol. 49, p. 3, 1968.

11. Bailey, R.J., and F.R. Cruickshank. "Applications of Infrared Fluorescence," Applied Spectroscopy Reviews. Vol. 10, p. 1, 1975.

12. Bernstein, L.S., F. Bein, D.C. Robertson, J.A. Jamieson, and D.R. Maley. "Remote Detection of Chemical Agents by Laser Initiated Non-Resonant Infrared Spectrosopy." ARCSL-CR-82054, U.S. Army Chemical Systems Laboratory, Aberdeen Proving Ground, MD, June 1983.

13. "Light Sources, Monochromators, and Detection Systems--Vol. 2." Oriel Inc., Stratford, CT, p. 7, 1985.

14. "Light Sources Monochromators, and Detection Systems--Vol. 2." Oriel Inc., Stratford, CT, pp. 30, 128; 1985.

15. Dolphin, D., and A. Wick. "Tabulation of Infrared Spectra," Wiley Interscience. New York, p. 530, 1977.

16. Flanigan, D.F. "The Spectral Signatures of Chemical Agents Vapors and Aerosols." CRDEC-TR-84061, U.S. Army Chemical Research, Development, and Engineering Center, Aberdeen Proving Ground, MD, July 1985.

17. Robinson, J.W., C. Woodward, and H.M. Barnes. "Detection of Gaseous Organic Compounds by the Infrared Emission Stimulated by a Laser Beam," Analytica Chimica Acta. Vol. 43, p. 119, 1968.

18. Robinson, J.W., and N. Katayama. "Laser-Induced IR Fluorescence Spectra of Ethylene, Propylene, 1-Butene, Ethyl Acetate, Acetaldehyde, Ethyl Ether, Methyl Alcohol, and Ethyl Alcohol," Spectroscopy Letters. Vol. 7, p. 581, 1974.

APPENDIX A:

CALIBRATION OF THE MONOCHROMATOR-DETECTOR RESPONSE AT 8 μm.

INTENTIONALLY LEFT BLANK.

The following calculation determines both the spectral power at a wavelength of 8 μm that the glowbar deposits on the monochromator entrance slit and the fraction of this flux which eventually passes through the monochromator to the HgCdTe detector at the exit slit. The optical layout of the glowbar and monochromator is shown in Figure 2. The numerical values of those quantities critical in the calculation are from Reference 13 and the test geometry. They are as follows:

1. IR glowbar active area (6 mm x 20 mm) (A) . . . . . 120 mm^2
2. IR glowbar 8-μm spectral irradiance at a 50-cm distance per 10-mm^2 emitter area (E_λ) . . . . . 2.4 x 10^{-3} mW/cm^2-μm
3. Illuminator mirror area (a) . . . . . 40.32 cm^2
4. Illuminating mirror--glowbar separation (r) . . . . . 13.3 cm
5. Entrance slit area (0.6 mm x 12 mm) . . . . . 7.2 mm^2
6. Detector area (1 mm x 1 mm) . . . . . 1.0 mm^2
7. Monochromator bandpass . . . . . 0.061 μm
8. Combined preamplifier gain . . . . . 518.

Noting that the glowbar spectral irradiance is given in terms of a fixed distance of 50 cm and a 10 mm^2 emitting area, we must first correct it for the present geometry. The spectral power P_m incident on the surface of the illuminating mirror at 8 μm is given by:

$$P_m = E_\lambda \left(\frac{A}{10\ mm^2}\right) \left(\frac{50\ cm}{r}\right)^2 a \qquad \text{(A-1)}$$

or P_m = 16.41 mW/μm. The concave mirror in the illuminator provides a 1.8X magnified image of the glowbar on the entrance slit. The size of the glowbar image at the entrance slit becomes 10.8 x 36 mm, and its area is 388.8 $mm.^2$ The vignetting factor, due to the size of the slit, is the ratio of the slit-to-image areas or 0.0185. The spectral power P_s through the slit is then the product of the incident power on the mirror from Equation A-1, a factor of 0.9 for reflection (10-percent loss from the mirror) and the vignetting factor or 0.273 mW/μm.

Once the flux enters the slit, the fraction, following a path which ultimately falls on the sensitive portion of the HgCdTe detector, is equal to the ratio of the area of the entrance slit

(0.6 mm x 12 mm) to the area of the exposed portion of the detector's active element (0.6 mm x 1 mm) or 0.0833. The detectable spectral power at 8 μm through the entrance slit is thus the product of the spectral power through the entrance slit and this fraction or 22.8 μW/μm. One must now consider the dispersive effects of the monochromator. Its bandpass is 0.061 μm at 8 μm. Accordingly, the spectral power occurring within the bandpass is given by the product 22.8 μW/μm and 0.061 μm or 1.39 μW.

The throughput of the monochromator must now be taken into account. There are losses resulting from the differing focal ratios of the f/3.4 glowbar source illuminator mirror coupling to the f/3.7 monochromator mirror (14 percent), in the reflection at each of the four reflecting surfaces within the monchromator (10 percent each) and in its reflection from the grating (50 percent at blaze). The power surviving the monochromator is 0.39 μW. Remembering that the glowbar and fluorescent signals are chopped with a square wave that modulates the signal to a 50-percent root mean square delivered power, we may conclude that power, which ultimately arrives upon the detector sensitive element from the glowbar, is 0.195 μW.

The value given above may be verified by referring to the HgCdTe detector's response to a 500°K blackbody. Data provided by the detector's manufacturer, EG&G Judson Inc., gives a responsivity in this case of 717 V/W. From Figure 4 we find that the detector produced 80 mV at 8 μm. After the gain of the preamplifiers and the responsivity are factored in, the power incident on the detector becomes 0.215 μW--a number that is close to the value above. Since the responsivity at 8 μm is likely to be at least slightly different from the 500° K blackbody value we have used, the close agreement is probably somewhat fortuitous, but it gives us confidence in our calibration calculation.

A second method was also used to verify the calibration method. The HgCdTe detector was replaced with an Oriel Model 7080 pyroelectric radiometer. Under conditions identical to those used in calibration, a power of 0.25 ± 0.1 μW was observed at a 3.7-cm distance behind the exit slit. Knowing the flux exiting the slit of the monochromator will diverge in a f/3.7 cone, the power value measured by the radiometer separated from the exit slit is in sufficient agreement to reinforce our calculated value (0.39 μW).

APPENDIX B:
CALCULATION OF THE SPECTRAL RADIANCE OF THE FLUORESCING GAS

INTENTIONALLY LEFT BLANK.

In this appendix we shall develop an expression which provides the geometrical connections needed to derive a physical property of the fluorescing gas, i.e., its spectral radiance, from measurements of the amount of power passing through the monochromator entrance slit.

The geometry of the fluorescing column illuminated by the laser is given in Figure B-1. Let us now make the following identifications:

P_s = The spectral power through the entrance slit of the monochromator in milliwatts/micron

y = Distance from the center of the viewable portion of the beam to the center of the monochromator entrance slit (37.5 mm)

d = The slit width in millimeters

b = The beam diameter

$\Re_v$ = The volume spectral radiance of the fluorescing gas in milliwatts/microns - steradian - cubic centimeters

x_o = The distance from the center of the viewable portion of the beam to its axial extremities (11 mm)

l = The monochromator slit length (12 mm) .

Consider the viewable portion of the beam (shaded) and a differential segment of its volume located at a distance x from its center. The amount of power entering the monochromator slit from a differential volume of emitting gas is given by the product of the volume's spectral radiance, the volume of that emitting region dV, and the solid angle Ω the entrance slit subtends as viewed from the differential volume or:

$$P_s = \Re_v dV\Omega \; . \tag{B-1}$$

From Figure B-1, we know $dV = \pi(b/2)^2\, dx$ and $\Omega = ld / (y^2 + x^2)$. The total power is obtained by integrating over the entire visible column, which by symmetry can be reduced as follows:

$$P_s = \int_{-x_o}^{x_o} \frac{\Re_v l d\pi b^2 dx}{4(y^2 + x^2)} = \int_{o}^{x_o} \frac{\Re_v l d\pi b^2 dx}{2(y^2 + x^2)} \; . \tag{B-2}$$

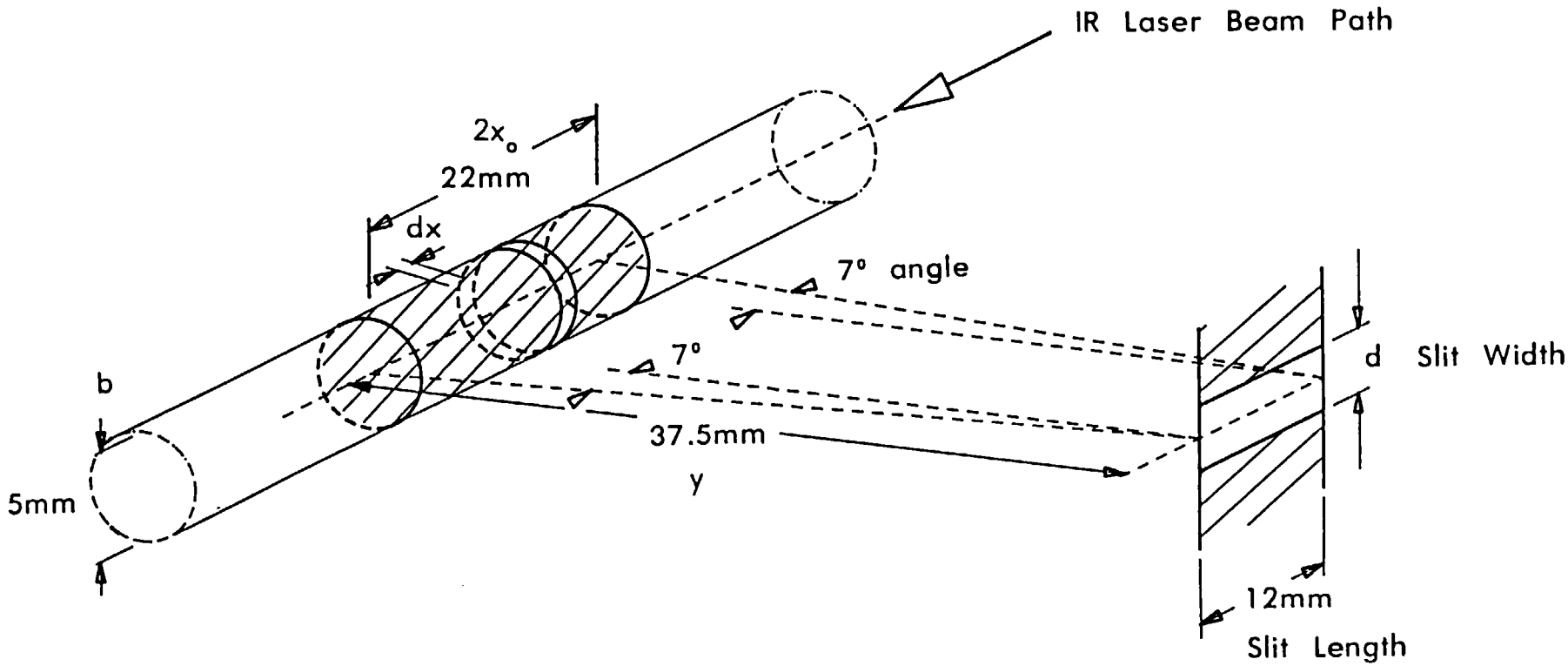

Figure B-1. Geometry of the fluorescing column of vapor illuminated by the laser in front of the monochromator slit.

The above, of course, uses the approximating assumption that the beam diameter is small compared to the beam-slit distance, i.e., that all the flux from the differential volume may be considered to come from its center. Introducing the further approximation that the solid angle subtended by the entrance aperture is uniform for all viewable points on the beam, we find the integral becomes:

$$P_s = \Re_v \frac{l d \pi b^2}{2} \int_0^{x_o} \frac{dx}{(y^2 + x^2)} \quad . \tag{B-3}$$

The above integrand is solvable analytically and has a solution:

$$P_s = \Re_v \frac{l d \pi b^2}{2} \tan (x_o/y) \quad . \tag{B-4}$$

When the above equation is inverted to solve for $\Re_v$, and substituting in the appropriate numerical values:

$$\Re_v \left(\text{mW}/(\mu\text{m - steradian - cm}^3)\right) = \frac{2.789 \times 10^3}{d\ (\text{mm})} P_s\ (\text{mW}/\mu\text{m}) \tag{B-5}$$

Note that, in keeping with convention, the expression is mixed mode--that is, the volume is expressed in cubic centimeters, and the slit width is given in millimeters. Note further that if the approximations used in arriving at Equation B-4 are not used, an exact integral description is still possible. Its solution, involving triple integrals, varies by only a few percent from the value above.

INTENTIONALLY LEFT BLANK.

No of Copies	Organization
1	Office of the Secretary of Defense OUSD(A) Director, Live Fire Testing ATTN: James F. O'Bryon Washington, DC 20301-3110
(Unclass., unlimited) 12 (Unclass., limited) 2 (Classified) 2	Administrator Defense Technical Info Center ATTN: DTIC-DDA Cameron Station Alexandria, VA 22304-6145
1	HQDA (SARD-TR) WASH DC 20310-0001
1	Commander US Army Materiel Command ATTN: AMCDRA-ST 5001 Eisenhower Avenue Alexandria, VA 22333-0001
1	Commander US Army Laboratory Command ATTN: AMSLC-DL Adelphi, MD 20783-1145
2	Commander Armament RD&E Center US Army AMCCOM ATTN: SMCAR-MSI Picatinny Arsenal, NJ 07806-5000
2	Commander Armament RD&E Center US Army AMCCOM ATTN: SMCAR-TDC Picatinny Arsenal, NJ 07806-5000
1	Director Benet Weapons Laboratory Armament RD&E Center US Army AMCCOM ATTN: SMCAR-CCB-TL Watervliet, NY 12189-4050
1	Commander US Army Armament, Munitions and Chemical Command ATTN: SMCAR-ESP-L Rock Island, IL 61299-5000
1	Commander US Army Aviation Systems Command ATTN: AMSAV-DACL 4300 Goodfellow Blvd. St. Louis, MO 63120-1798

No of Copies	Organization
1	Director US Army Aviation Research and Technology Activity Ames Research Center Moffett Field, CA 94035-1099
1	Commander US Army Missile Command ATTN: AMSMI-RD-CS-R (DOC) Redstone Arsenal, AL 35898-5010
1	Commander US Army Tank-Automotive Command ATTN: AMSTA-TSL (Technical Library) Warren, MI 48397-5000
1	Director US Army TRADOC Analysis Command ATTN: ATAA-SL White Sands Missile Range, NM 88002-5502
(Class. only) 1	Commandant US Army Infantry School ATTN: ATSH-CD (Security Mgr.) Fort Benning, GA 31905-5660
(Unclass. only) 1	Commandant US Army Infantry School ATTN: ATSH-CD-CSO-OR Fort Benning, GA 31905-5660
1	Air Force Armament Laboratory ATTN: AFATL/DLODL Eglin AFB, FL 32542-5000
	Aberdeen Proving Ground
2	Dir, USAMSAA ATTN: AMXSY-D AMXSY-MP, H. Cohen
1	Cdr, USATECOM ATTN: AMSTE-TD
3	Cdr, CRDEC, AMCCOM ATTN: SMCCR-RSP-A SMCCR-MU SMCCR-MSI
1	Dir, VLAMO ATTN: AMSLC-VL-D

No. of Copies	Organization
2	SRI International ATTN: Dr. M. Coggiola Dr. T.G. Slanger 333 Ravenswood Avenue Menlo Park, CA 94025
1	Commander US Army Atmospheric Sciences Laboratory ATTN: SLCAS-AE, Dr. F. Niles White Sands Missile Range, NM 88002-5501
	Aberdeen Proving Ground
10	Cdr, CRDEC, AMCCOM ATTN: SMCCR-DDT, Dr. R.A. Mackay SMCCR-RSL, Dr. A.P. Force Dr. S. Christesen Dr. C.S. Harden L. Hoffland Dr. S.R. Long SMCCR-RSP, A.K. Stuempfle SMCCR-RSP-B, D.F. Flanigan SMCCR-RST-C, Dr. S. Thomson SMCCR-TD, J.J. Vervier

USER EVALUATION SHEET/CHANGE OF ADDRESS

This Laboratory undertakes a continuing effort to improve the quality of the reports it publishes. Your comments/answers to the items/questions below will aid us in our efforts.

1. BRL Report Number BRL-TR-3096 Date of Report APRIL 1990

2. Date Report Received _____

3. Does this report satisfy a need? (Comment on purpose, related project, or other area of interest for which the report will be used.) _____

4. Specifically, how is the report being used? (Information source, design data, procedure, source of ideas, etc.) _____

5. Has the information in this report led to any quantitative savings as far as man-hours or dollars saved, operating costs avoided, or efficiencies achieved, etc? If so, please elaborate. _____

6. General Comments. What do you think should be changed to improve future reports? (Indicate changes to organization, technical content, format, etc.) _____

CURRENT ADDRESS

Name

Organization

Address

City, State, Zip Code

7. If indicating a Change of Address or Address Correction, please provide the New or Correct Address in Block 6 above and the Old or Incorrect address below.

OLD ADDRESS

Name

Organization

Address

City, State, Zip Code

(Remove this sheet, fold as indicated, staple or tape closed, and mail.)

---FOLD HERE---

DEPARTMENT OF THE ARMY
Director
U.S. Army Ballistic Research Laboratory
ATTN: SLCBR-DD-T
Aberdeen Proving Ground, MD 21005-5066
OFFICIAL BUSINESS

NO POSTAGE
NECESSARY
IF MAILED
IN THE
UNITED STATES

BUSINESS REPLY MAIL
FIRST CLASS PERMIT No 0001, APG, MD

POSTAGE WILL BE PAID BY ADDRESSEE

Director
U.S. Army Ballistic Research Laboratory
ATTN: SLCBR-DD-T
Aberdeen Proving Ground, MD 21005-9989

---FOLD HERE---